NTNU – Trondheim
Norwegian University of
Science and Technology

Iron oxide nanocrystals clustered in oil-in-water nanoemulsions: Preparation, characterization, and transverse relaxivities

Hailay Teklegiorgis Hadera

MSc in Physics
Submission date: June 2015
Supervisor: Pål Erik Goa, IFY
Co-supervisor: Sjoerd Hak, IFY

Norwegian University of Science and Technology
Department of Physics

Acknowledgements

I am heartily thankful to my supervisor Pål Erik Goa (Associate Professor), whose encouragement, guidance and support from the start to the finish level enabled me to develop an understanding of the project. His all rounded guidance helped me a lot. I also would like to express my sincere gratitude to my co-supervisor Sjoerd Hak (PhD) for his patience, motivation and enthusiasm. He has made available his endless support in a number of ways.

Then I want thank the staffs at the biophysics and MR center for their help in the laboratory works. My sincere thanks also goes to the department of Physics for making my stay pleasant at the department.

Last but not least, I offer my regards and blessings to all my family and friends specially Hagos Gebrehiwot for his tutor on LATEX and everyone who supported me in any aspect during the completion of the thesis work.

Symbols and Abbreviations

MRI	Magnetic resonance imaging
IONCs	Iron oxide nanocrystals
NEs	nanoemulsions
RF	Radio Frequency
TE	Echo Time
CPMG	Carr-Purcell-Meiboom-Gill
DLS	Dynamic light scattering
ICP-MS	Inductively coupled plasma mass spectrometry
TEM	Transmission Electron Microscopy
ω_0	Lamor frequency
γ	magnetogyric ratio
η	viscosity
TR	Repetition Time
$[CA]$	Contrast agent concentration
T_1	Longitudinal relaxation time
T_1	Transverse relaxation time
R_1	Longitudinal relaxation rate
R_2	Transverse relaxation rate
r_1	Longitudinal relaxivity
r_2	Transverse relaxivity
DSPC	Di-stearoyl-phospho-choline
PEG-DSPE	di-stearoyl-phosphatidyl-ethanolamine-N-methoxy(polyethylene glycol)-2000
τ_D	Translational diffusion time
$\delta\omega$	angular frequency shift
L	Langevin function
$\mu_c r$	magnetic moment of the IONC
B_{eq}	equatorial field
R_{LA}	Radius of the loose aggregates
R_{hdr}	hydrodynamic radius
l_{PEG}	PEG thickness
R_{DA}	Radius of the aggregates

τ_m	Residence time
C_T	bulk proton concentration
PDI	polydispersity index
O/W	Oil-in-water
W/O	water-in-oil

Constants with their values and units

constant	symbol	value	unit
water diffusion constant at 40^oC	D	3×10^{-9}	m^2s^{-1}
water diffusion constant at 24^oC	D	2.3×10^{-9}	m^2s^{-1}
Avagadro's constant	NA	6.02214×10^{23}	mol^{-1}
vacuum permeability	μ_0	$4\pi \times 10^{-7}$	NA^{-2}
Boltzmann's constant	K_B	1.38065×10^{-23}	JK^{-1}

Abstract

Iron oxide nanocrystals (IONCs) have attracted extensive interest due to their high magnetization that efficiently decreases the transverse relaxation times of water protons. The increase in their transverse relaxivities upon crystal clustering is also considered as one of their important properties.

Nanoemulsions (NEs) were developed with oil-in-water emulsions containing IONCs in an oil core stabilized by phospholipids (DSPC) and di-stearoyl-phosphatidyl-ethanolamine-N-methoxy(polyethylene glycol)(PEG-DSPE) lipid amphiliphiels. We prepared two different NEs: NEs containing 10 mol% and 50 mol% PEG2000-DSPE (P10 and P50), while their sizes were kept constant. Monodisperse aggregates for P10 and unevenly dispersed IONCs for P50 batches were developed.

IONCs-loaded NEs were analyzed by Dynamic light scattering (DLS) to obtain the hydrodynamic diameter, Inductively coupled plasma mass spectrometry (ICP-MS) to measure iron concentration, and Transmission Electron Microscopy (TEM) to observe the IONCs in the NEs. Furthermore, transverse relaxivities, r_2 were measured at 0.47 T, 1.5 T, 3 T and 7 T.

The experimental relaxivities were interpreted based on two parameters: the number of IONCs in each droplet and the magnetic field strengths. Experimental relaxivities of P10 NEs were in good agreement with the theoretical studies. Relaxivities increased with increased number of IONCs in each droplet and relaxivities increased with increased magnetic field until they level of when magnetization saturation has been attained. Experimental relaxivities of P50 were close to the prediction of the static dephasing regime model and much higher than the fast diffusion model predictions.

In the current work it is evident that there is a significant difference in the experimental relaxivities of P10 and P50 batches. However, due to the difference in geometry between P10 and P50, we are not able to make conclusions about the effect of PEG density. A thorough preparation and characterization of NEs with a numerical simulation may be needed to explain the effect of PEG density.

Contents

1 Introduction

Magnetic resonance imaging (MRI) is a non-invasive imaging modality, which is widely used for clinical and research applications. Its ability to provide detailed images of soft tissues is considered as its substantial advantage compared to other imaging techniques [1]. MRI is a renowned technique with its excellent intrinsic contrast, which is generated on the basis of tissue difference in proton density, T_1 and T_2 relaxation times of the tissues [2]. However, the native contrast between different tissues is not always enough for specific applications. In order to enhance the contrast between different tissues, it requires the use of extrinsic contrast agents. These contrast agents increase the contrast with the surrounding tissue by locally shortening T_1 and T_2^* relaxation times and can be categorized as T_1 and T_2^* contrast agents [2].

One category of contrast agents that mainly shorten T_1 relaxation time are considered as positive contrast agents (appearing bright on MRI), usually composed of paramagnetic metal ions, typically of the Gd^{3+} ion. These contrast agent will not be discussed in this work. A second class of contrast agents, on which this thesis will focus, is that of superparamagnetic nanoparticles, usually iron-oxide based, which can be considered as negative agents (appearing predominantly dark on MRI) for MRI [2]. Iron oxide nanocrystals (IONCs) with a typical core diameter in the order of 4-50 nm are top of current interest due to their application in the field of nanomedicine [1–3].

The IONCs have attracted extensive interest due to their high magnetization that efficiently decreases the transverse relaxation times of water protons and leads to negative contrast [4]. The increase in their transverse relaxivities upon crystal clustering is also considered as one of their important properties [5]. Various studies have discussed the effect of clustering on IONCs relaxivity [4–6], and more specifically Vuong et al. described it by theoretical models and computer simulations [6]. Studies have proven that computer simulations have successfully validated theoretical models while experimental data have shown less degree of agreement with the theoretical model results [6,7]. Though experimental studies are less numerous than studies with computer simulations, the comparison between experimental results

and theoretical models is top priority to optimize the contrast agent's relaxivity [5].

The research activity on the preparation and application of nanoparticles for nanomedicine has been growing during recent years [8]. Lipid-based nanoparticles, such as nanoemulsions (NEs), are increasingly studied for drug delivery and molecular imaging purposes. Furthermore, studies on the incorporation of contrast generating materials in lipid-based nanoparticles for imaging purposes have also increased.

The starting point for this master thesis is a previous work performed by Hak et.al where nanoemulsions of IONCs were synthesized and the experimental transverse relaxativity was compared to model predictions [4]. The results showed that the transverse relaxivity was significantly higher than predicted from fast diffusion models. One possible mechanism which could offer an explanation for these results is exchange of water protons between a static region in the vicinity of the surface of the NE and a dynamic averaging (fast diffusion) regime in the bulk water. The study has hypothesized the relaxivity should increase with the thickness of the polyethylene glycol (PEG-2000) coating. The experimental results did not agree with model predictions. Water diffusion relative to the nanoparticles is a crucial parameter. The nanoemulsions in that study were coated with a relatively thick and dense PEG layer, this may affect water diffusion around the nanoparticle. That study hypothesized that the polyethylene glycol coating on the nanoparticles was causing the deviation.

Therefore, the purpose of this master thesis was two fold; first to synthesize oil-in-water emulsions containing IONC clusters with a controlled nanoemulsion size and IONC loading , and most importantly to vary the surface layer thickness to vary the exchange volume; second to measure the experimental transverse relaxivity values and see if the results are consistent with the proposed exchange hypothesis.

2 Theory

2.1 Magnetic Resonance Imaging

Magnetic resonance imaging is one of the most important imaging techniques in clinical diagnostics and medical research [9]. Its flexibility and sensitivity to a wide range of tissue properties makes it a powerful imaging technique [10]. The noninvasive nature of the magnetic fields employed has given an extra edge in terms of safety compare to other imaging modalities.

MRI exploits the equilibrium net nuclear magnetization that is emerged as a consequence of the tiny imbalance in the spin-up and spin-down protons when water molecules are introduced in a magnetic field [2]. According to the classical explanation of NMR, these nuclei can be thought of as having tiny spins that precess in the presence of an external magnetic field. The precession frequency (Lamor frequency) of the nuclear spins (ω_0) is directly proportional to the strength of the external applied magnetic field and given by the equation [11]:

$$\omega_0 = \gamma B_0, \tag{2.1}$$

where B_0 is the strength of the applied magnetic field and γ is magnetogyric ratio and it differs for different nuclei (i.e for ^1H, $\frac{\gamma}{2\pi}$ =42.58 MHz per Tesla).

The net magnetization vector can be excited by applying radio frequency (RF) pulse with a frequency that matches the Larmor frequency [2]. After the RF introduction, the equilibrium magnetization is flipped down into a plane perpendicular to the external magnetic field. Hence the magnetization can precess around the equator plane with the same frequency as the induced RF-pulse and the rotation depends on the strength and duration of the induced RF-pulse [2].

Magnetic resonance signals produced from hydrogen nuclei found in water molecule and the signals are recorded as induction voltage in receiving coils placed perpendicular to the external magnetic field. When the RF is tuned into resonance, the protons will be excited from one state to the other state and there are forces that

drive the magnetization of the protons to back to their equilibrium position and such a process is called relaxation process [2].

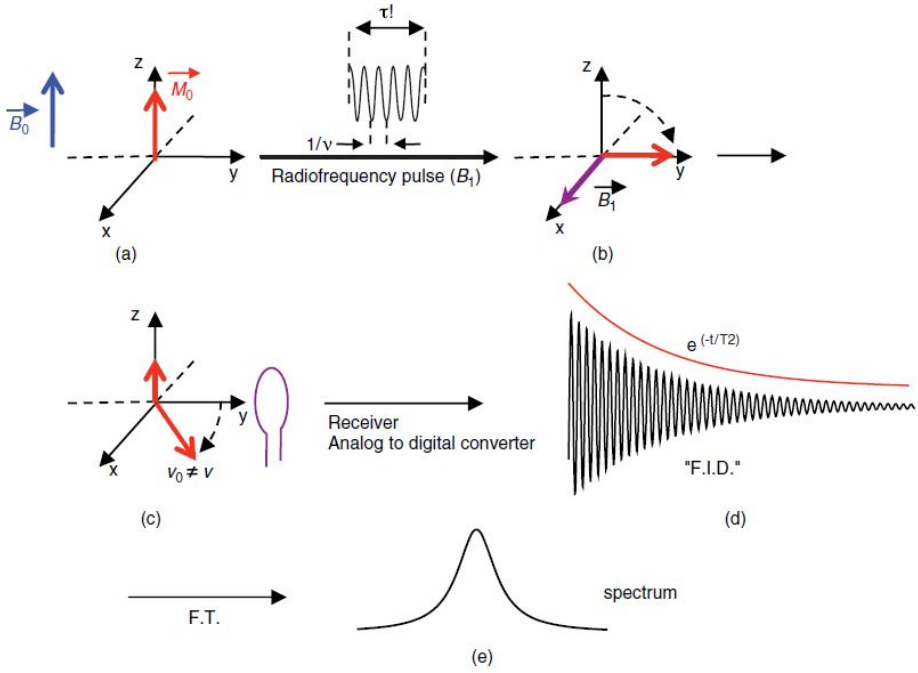

Figure 2.1: (a) net magnetization M_0 at equilibrium when the spins are placed in a permanent magnetic field B_0; (b) RF pulse, induced by a perpendicular B_1 magnetic field created by an RF coil, flips the magnetization into the xy plane; (c) the magnetization M precesses around the z axis and the signal decreases in the xy plane; (d) Free Induction Decay (FID): the recorded signal is a damped sinusoid; (e) NMR spectrum produced by a Fourier transform [9]. Reprinted with permission

2.1.1 Relaxation

The relaxation process is analyzed in terms of different independent processes, T_1, T_2 and T_2^* processes [10]. T_1 relaxation, is characteristic of the recovery to equilibrium of the magnetization, M_z after the excitation pulse. Whereas T_2 relaxation is characteristic of the fade of the signal in the xy plane [2, 9]. Another relaxation time is T_2^*, a combination of T_2 and the contribution of all external magnetic field inhomogeneities and related to specific properties of the sample $T_2^{'}$ [9]. Block equation proposed an expression to quantify the relaxation process in terms of the relaxation times T_1 and T_2 [9]. The magnetization M_0 is the equilibrium value of M_z and when the RF-pulse is applied, M_x and M_y relax to zero while M_z relaxes

to M_0.

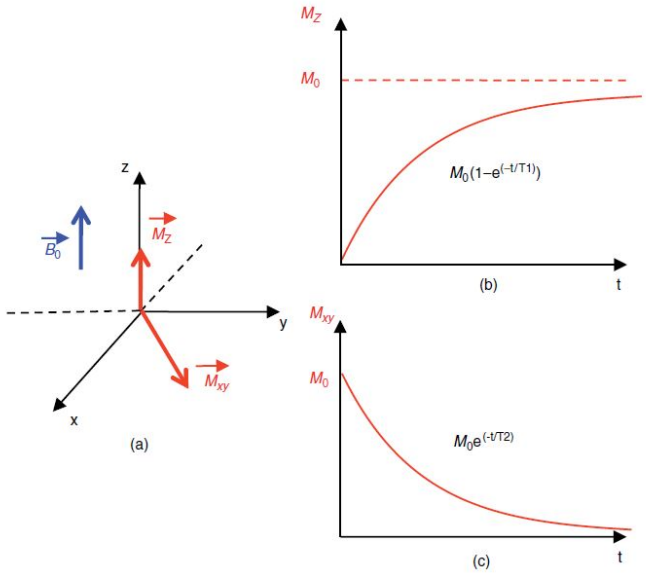

Figure 2.2: (a) Return to equilibrium of the magnetization, (b) return to equilibrium on the z axis,(c) return to equilibrium in the xy plane [9]. Reprinted with permission

2.1.2 Spin-lattice relaxation

The spin-lattice relaxation is characterized by T_1 that measures the rate of transfer of energy from the nuclear spin environment to the neighboring molecules [9]. After excitation of the nuclear magnetization by RF-pulse, the excited nucleus has involved in an enthalpic interaction with its environment, in particular with the magnetic active agents of its environment [2, 11]. The spin lattice relaxation is the responsible one for the returning of the magnetization, M_z to the equilibrium magnetization M_0 with time t according to:

$$\frac{dM_z}{dt} = \frac{M_0 - M_z}{T_1}, \tag{2.2}$$

where T_1 is the longitudinal relaxation time and the general solution of the differential equation is given below:

$$M_z = M_0(1 - e^{\frac{-t}{T_1}}). \tag{2.3}$$

2.1.3 Spin-Spin Relaxation

This is an entropy interaction that leads to the spin dephasing in the xy plane [9,11]. The entropy causes for the transverse magnetization, M_xy and decay with time t. The decay rate of transverse relaxation is given as:

$$\frac{dM_{xy}}{dt} = \frac{-M_0}{t}, \tag{2.4}$$

where T_2 is the transversal relaxation time that characterizes the disappearance of the signal in the xy plane and the general solution of the differential equation 2.4 is given by [2]:

$$M_{xy} = M_0 e^{\frac{-t}{T_2}}. \tag{2.5}$$

The dephasing of the spins occurs when the nuclear moment of the spins experiencing a modulated dipole field produced by its surroundings. From this, the individual spin will experience different total magnetic field. The difference of magnetic field leads to precess at different resonance frequency during oscillates in the transverse plane. A kind of variations is caused not only by macroscopic inhomogeneities but it is also caused by microscopic fluctuations in the local field. The total contribution of the microscopic (dipolar), T_2 and macroscopic, $T_2^{'}$ represented by accelerated transversal relaxation, T_2^* and given by [2, 11]:

$$\frac{1}{T_2^*} = \frac{1}{T_2} + \frac{1}{T_2'}. \tag{2.6}$$

T_2 and T_2^* relaxation times can be differentiated by specific detection sequences.

2.1.4 Basic pulse sequences

An MRI sequence is a combination of series of RF-pulses, gradients, and time intervals, which can be put together to detect the proton relaxation in MRI [10]. The MR signals are recorded as induction voltages in receiver coils. In essence, the signal and the contrast can be optimized by changing the sequence parameters. The basic components of MRI sequences are RF-pulses: for spin excitation, magnetic field gradients: for the spatial encoding of the signal in the k-space and an acquisition period: to record the echoes signal with a defined contrast. Spin echo is one of the commonly used sequences.

Spin echo sequences: The spin echo sequence is based on the application of two RF-pulses: 90^o-pulse followed by 180^o-pulse [10]. The 90^o and 180^o pulses are used for the excitation and refocusing pulses and applied at echo time (TE)=0 and TE/2 respectively. The process is repeated at repetition time, TR intervals. The refocusing pulse (180^o) allows permanent field inhomogeneities to be compensated for and produces an echo signal weighted by T_2 relaxation time [9]. The spin

echo sequence can be a single echo sequence or multi-echo sequence. Instead of repeating an experiment with a different echo time to measure T_2, it is common to use multiple spin echo sequence, which collect data for more than one echo of the original RF excitation by applying multiple 180^o-pulses after a single 90^o-pulse [10].

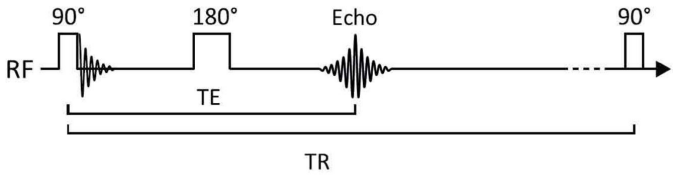

Figure 2.3: Spin echo sequence diagram

2.1.5 Contrast agents

Based on the desired application, the inherent soft-tissue contrast is good enough to discriminate different tissues on MRI [2, 9]. The inherent soft-tissue contrast is generated on the basis of local difference of the intrinsic physical parameters T_1, T_2, T_2^* and proton density [10]. However, the intrinsic contrast between different tissues is limited to differentiate the normal and diseased tissues. For this reason, MRI required to use contrast agents to improve the contrast between normal and diseased tissues [3].

The purpose of using a contrast agent in MRI is to decrease the relaxation times of water protons in the surrounding tissue [9]. They create a strong non uniform magnetic field in the environment to accelerate the relaxation of water protons in their vicinity.

The influence of a contrast agent to reduce the relaxation times for a specific concentration [CA] is called the relaxivity of the agent and is expressed by [3]:

$$R_i = R_{i,tissue} + r_i[CA], \tag{2.7}$$

where i$\epsilon\{1, 2\}$, R (s^{-1})is the relaxation rate, $R_{,tissue}$ is the intrinsic relaxation rate of the tissue, r (mMs^{-1}) is the relaxivity and [CA] (mM) is the the contrast agent concentration. From equation 2.7 the relaxivity of the contrast agent is determined from a graph of relaxation rate versus [CA] and the slop of the graph represents the relaxivity of a given contrast agent.

Based on the relaxivity ratio,r_2/r_1, the contrast agent can be categorized as T_1, T_2 and T_2^* [3]: If, r_2/r_1 is in the range of 1-5, the agent is suitable as T_1 contrast agent, which mainly accelerates T_1 that leads to increase signal intensity (positive

contrast) [2]. T_1 contrast agents are mainly paramagnetic metal ion containing agents usually Gd^{3+} [3]. If, r_2/r_1 is larger than 5, the agent is suitable as T_2 or T_2^* contrast agent, which mainly accelerates T_2 or T_2^* that leads to reduce signal intensity (negative contrast) [2]. T_2 contrast agents are mainly superparamagnetic metal ion containing agents commonly iron oxide nanoparticles.

Superparamagnetic contrast agents "Superparamagnetic nanoparticles are coated nanocrystals of iron oxides, characterized by a large magnetic moment in the presence of a static external magnetic field" [12]. These nanoparticles exert strong reduction in the T_2 or T_2^* relaxation times. Magnetite (Fe_3O_4) and maghemite (γFe_2O_3) with a core diameter in the range of 4-50 nm [3] are among the commonly used iron oxide nanoparticles for MRI contrast. The magnetite is a ferrimagnet with a crystallographic inverse spinel structure and a saturation magnetization of 510kA/m [2]. The factors that affect the efficiency of superparamagnetic nanoparticles are the size of the crystals, the charge, the nature of the coating and the hydrodynamic size of the coated particle [12]. IONCs, on which this thesis was used, are also widely used as MRI contrast agents due to their localized reducing transverse relaxation time [4, 12].

Nanoemulsions (NEs): An emulsion is a mixture of two or more immiscible liquids and they are dispersed one in the other [13]. Oil-in-water (O/W) and water-in-oil (W/O) are the two common emulsions. The oil is the phase that dispersed in oil-in-water emulsion while water is the continuous. These oil droplets are subsequently stabilized by amphiphiles, which contain polar and non-polar domains, to create small particles in the range of 30-100 nm [13] and with narrow size distributions [14]. NEs are used as formulations of nanoparticles for a contrast agent and drug delivery applications [14].

Lipid amphiliphiels such as di-stearoyl-phospho-choline (DSPC) and di-stearoyl-phosphatidyl-ethanolamine-N-methoxy(polyethylene glycol)(PEG-DSPE) are widely used in emulsions. The DSPC is used to create stable oil-in-water emulsion while the PEG-DSPE used to improve the biocompatibility, increase the circulation time and increase the stability [8, 15].

The NEs used in this thesis were oil-in-water NEs. The contrast agent iron oxide was also incorporated into the NE, schematically illustrated in figure 2.4.

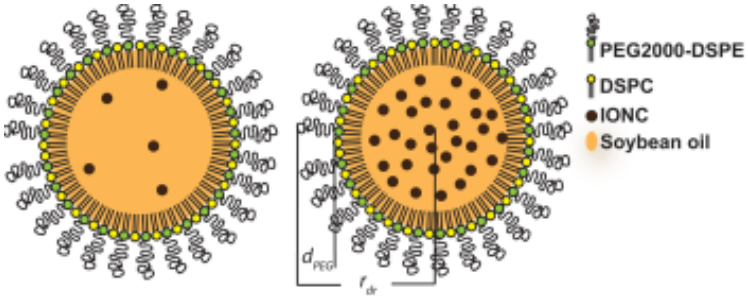

Figure 2.4: Schematic representation of nanoemulsions with low and high number of IONCs [4] Reprinted with permission.

2.2 Theoretical models for transverse relaxivity

Analyzing and understanding the execution of iron oxide as a contrast agents for MRI demands a theory that explains their magnetic interactions with water protons [16]. The main intention of understanding and identification of these relevant models is, to drive the dependency of the proton transverse relaxation rate (R_2) on the properties of the MR contrast agents.

The IONC contribution on the surrounding proton relaxation time can be explained as inner sphere and outer sphere models [4,17]. The contribution from inner sphere is emanated from the close contact of the protons and it is interaction with the electron spins of the superparamagnetic [2,4]. This exchange resulted from the dipolar interactions between the protons and the magnetic nanoparticle ions. As Hak et.al explained, the inner sphere relaxation for the IONC is considered as negligible as compared to the effect of outer sphere relaxation [4]. Brooks et.al also explained why the inner sphere relaxation is negligible, that is due to the low concentration of the fraction of protons that are bound and negligible dipolar and scalar interaction between the protons and the supermagnetic ions [1]. Whereas the outer sphere describes the relaxation induced by the diffusion of water protons within the inhomogeneous magnetic field created by the superparamagnetic particles [2, 4]. So that the magnetic dipolar interaction of the water proton with the inhomogeneous fields created by the IONC is the responsible one for the relaxation induced by the outer sphere [17].

The relaxation is described by the characteristic translational diffusion time (τ_D), the characteristic angular frequency ($\delta\omega$), a frequency which characterize the nuclear precession at the equatorial magnetic field of the particles and the volume fraction of magnetized particle, f. For nanoparticles with a radius r and water

diffusion constant D, τ_D can be defined as:

$$\tau_D = \frac{r^2}{D}, \tag{2.8}$$

where τ_D is the characteristic diffusion time required for a water molecule to diffuse a distance equal to the particle diameter [4] and this characteristic diffusion time determines the transitions between the relaxation regimes [18]. If τ_D is smaller than $\delta\omega$, the relaxation is expressed by the fast diffusion regime [19]. Since the particles are small, the relaxation rate in the inhomogeneous magnetic field is dominated by the nuclear diffusion with a validity condition:

$$\tau_D < \delta\omega^{-1}. \tag{2.9}$$

Since the echo time for aggregates which are not too large sizes, usual the echo times ($\tau_{cp} = TE/2TE$) are too long to be efficient, and there is no difference between T_2 and T_2^* on the fast diffusion regime.

If the above condition is not fulfilled, i.e., the time required to diffuse, τ_D between the IONC particles is longer than the resonant frequency offset, $\delta\omega^{-1}$ according to [2, 4, 6, 20]:

$$\tau_D > \delta\omega^{-1}. \tag{2.10}$$

This condition refers to the dephasing of motionless spin in an inhomogeneous field created by the magnetic particles.

2.2.1 Fast diffusion Regime

The T_2 relaxation time of freely diffusing bulk water is governed by the motional averaging regime with the relaxation rate ($R_2 = 1/T_2$) proportional to τ_D. Cowan, 1997 came to an expression, which shows the spin-spin relaxation time, T_2 is the reciprocal of the angular frequency shift, $\delta\omega$ [21]. According to Cowan, 1997, R_2 in terms of the the correlation time τ_D is given by the below expression [21]:

$$R_2 = \langle\omega_{loc}^2\rangle\tau_D, \tag{2.11}$$

where $\langle\omega_{loc}^2\rangle$ is the mean square dephasing frequency in the local magnetic field. From the above expression the relaxation rate in the fast diffusion regime for a super paramagnetic is derived according to [2, 4, 6, 20]:

$$R_2 = af(\delta\omega)^2\tau_D, \tag{2.12}$$

where a is a constant equal to $16/45$ for purely motional narrowing [17], f is the volume fraction occupied by IONC particles and given by:

$$f = N_{IONCs}(\frac{\frac{4}{3}\pi r^3}{V_{sample}}), \tag{2.13}$$

where N_{IONCs} is the number of IONC particles in the total volume V_{sample} [6], γ is the gyromagnetic ratio and $\delta\omega$ is defined as [2, 6]:

$$\delta\omega = \gamma B_{eq}, \tag{2.14}$$

where B_eq is the equatorial field at the particle equator and defined by [4, 6]:

$$B_{eq} = \frac{\mu_0 \mu_s}{4\pi R^3}, \tag{2.15}$$

where μ_0 is the vacuum magnetic permeability, μ_s is the magnetic moment of the IONCs and defined by [17]:

$$\mu_s = \frac{4\pi M_0 R^3}{3}. \tag{2.16}$$

Then according to [6, 20] the B_eq of the isotropically distributed spherical IONCs is given by:

$$B_{eq} = \frac{\mu_0 M_0}{3}, \tag{2.17}$$

where M_0 is the magnetization (magnetic moment per unit volume) of the IONCs and for isotropic then M_0 will be parallel to the applied external magnetic field, B_0 and given by [2, 21]:

$$M_0 = M_{cr} L, \tag{2.18}$$

where M_{cr} is the saturate magnetization of the IONCs and L is the Langevin function that relates the magnetization induced by paramagnetic particles and the applied external magnetic field B_0 at temperature T and defined as [2, 4]:

$$L = \coth(\frac{\mu_{cr} B_0}{K_B T}) - \frac{K_B T}{\mu_{cr} B_0}. \tag{2.19}$$

Note that $\mu_c r$ and k_B are the magnetic moment of the IONC and Boltz-man's constant respectively. Now by rewriting equation 2.17 the equatorial field for iron oxid nanocryastals can be describe as:

$$B_{eq} = \frac{\mu_0 M_{cr} L}{3}. \tag{2.20}$$

Then combining all the above equations, the relaxivity rate of isotropically distributed spherical IONCs in fast diffusion regime is given as:

$$R_2 = \frac{16}{45} f(\frac{\gamma \mu_0 M_{cr} L}{3})^2 \frac{r_{cr}^2}{D}, \tag{2.21}$$

with r_{cr} the radius of the iron oxide nanocrystal and R_2 is proportional with the transverse relaxivity, r_2, which is defined as the parameter of contrast agents that describes their ability to enhance at a given concentration. In a simple way r_2 is defined as the relaxation rate enhancement per millimole of iron [7]. Then the above transverse relaxation rate in the presence of a contrast agent can be rewritten as the following expression [2, 4]:

$$R_2 = R_{2,0} + r_2[CA], \tag{2.22}$$

where $R_{2,0}$ is the intrinsic relaxation rate of the medium in the absence of the contrast agent, it is negligible relative to R_2 and $[CA]$ is the concentration of the contrast agent in mM. The volume fraction, f can be expressed in terms of the Fe concentration [4, 22]:

$$V_{molar} = \frac{f}{[Fe]} = \frac{m_{Fe_3O_4}}{n_{Fe}\rho}, \tag{2.23}$$

where V_{molar} is the molar volume and $[Fe]$ at a given volume fraction f is determined by:

$$[Fe]^{FD}_{iso} = \frac{f}{\frac{4}{3}\pi r^3_{cr}} n_{Fe} = \frac{3f\rho}{m_{Fe_3O_4}}, \tag{2.24}$$

where n_{Fe} is the moles of Fe per IONCs, in this case $n_{Fe} = 3$, ρ is the density of iron oxide (Fe_3O_4) and $m_{Fe_3O_4}$ is the molar mass of Fe_3O_4. From equation 2.22 relaxivity, r_2 at a given Fe concentration is expressed by:

$$r_2 = \frac{R_2}{[Fe]}. \tag{2.25}$$

Finally by combining equations 2.21, 2.24 and 2.25 the relaxivity, r_2 of an isotropically distributed spherical IONCs at a given Fe concentration is given by the below expression [4]:

$$r_2 = \frac{16 m_{Fe_3O_4}}{1215\rho} (\gamma \mu_0 M_{cr} L)^2 \frac{r^2_{cr}}{D}. \tag{2.26}$$

The relaxivity can be calculated using the given parameters, which most of them are constants and others are related to the IONCs.

Transverse relaxation induced by agglomeration of IONCs

The size dependency of r_2 as shown on the above equation 2.26 is the motivation behind the study of the effect of particles' aggregation on r_2 . According to [7], the aggregation affects the transverse relaxivity due to the structure of the cluster and magnetic field distribution around the cluster. Studies have shown that the relaxation rate is dependent on the cluster geometry of the particles [2, 5, 6] and considering the aggregation of the particles as a single magnetized particle increases transverse relaxivity. In the motional averaging regime, the relaxivity, r_2 for different configuration of the aggregation is expressed as below.

Loose spherical aggregates

Here if the distribution of the particles in the sample considered as a uniform, the relaxivity can be determined by modifying equation(2.26) and introducing the radius of the loose aggregates, R_{LA}, the number of the particles in the aggregates, n_{cr}, the magnetization of the loose cluster, M_{LA} and the volume fraction, f.

In well-defined IONC clusters in NEs of water in oil, the radius R_{LA} is defined by [4]:

$$R_{LA} = R_{hdr} - l_{PEG}, \tag{2.27}$$

where, R_{hdr} is the hydrodynamic radius of the emulsion and l_{PEG} is the thickness of the PEG layer and can be calculated as [4]:

$$l_{PEG} = Na(\frac{a}{D})^{\frac{2}{3}}, \tag{2.28}$$

where N is the number of monomers per chain, a is the length of the monomer and D is the distance between the anchoring points of the PEG chains. (Note that these are constants and can be obtained from the specification of the different PEGs). The magnetization of the isotropically distributed spherical IONCs equation [23] can be adopted for the magnetization of the loose aggregation,M_{LA}:

$$M_{LA} = n_{cr} M_{cr} V_{rl} L, \tag{2.29}$$

with V_{rL} the volume ratio of the loose aggregate IONCs in the oil core and the total volume of the oil core which is considered as impenetrable sphere and given by:

$$V_{rl} = \frac{\frac{4\pi r_{cr}^3}{3}}{\frac{4\pi R_{LA}^3}{3}} = \frac{r_{cr}^3}{R_{LA}^3}. \tag{2.30}$$

Similarly equation (2.24) is modified for the loose aggregates as follows:

$$[Fe] = \frac{3f\rho}{m_{Fe_3O_4}} n_{cr} V_r. \tag{2.31}$$

After having all the above expressions the transverse relaxivity, r_2 for the loose aggregation is given by [4, 7]:

$$r_2^{LA} = \frac{16}{1215} \frac{m_{Fe_3O_4} n_{cr} r_{cr}^3}{\rho R_{LA} D} (\gamma \mu_0 M_{cr} L)^2. \tag{2.32}$$

Dense spherical aggregate

In dense aggregate, a spherical cluster with radius R_{DA} is a dense aggregate composed of n_{cr} iron-oxide particles confined in a small volume compare to the loose aggregate. The effective magnetization of the aggregate and the resulting frequency, $\delta\omega$ is proportional to the number of particles within the aggregate volume [2]. Here defining the exact radius of the aggregate is the main difficulty. However according to the Kepler conjecture [23], packing of spherical objects in euclidean three spaces has a smallest possible volume and a maximum density of around $\pi/\sqrt{18}$. Another study has also suggested that the maximum density is achieved when a sphere of radius R occupies a cube with a length 2R [6]. In this case the former assumption

is more convenient to have a minimum volume. If the assumption of the shape of the overall aggregate is spherical, then according to the theorem [23], the volume of the dense aggregate with n_{cr} of IONCs is given by:

$$V_{DA} = n_{cr}\frac{4}{3}\pi r_{cr}^3 V_{rD}, \tag{2.33}$$

where V_{rD} is the volume fraction of the dense aggregate equal to $\pi/\sqrt{18}$ and the radius of the spherical dense aggregate, R_{DA} can be determined using equation (2.33):

$$R_{DA} = \sqrt[3]{\frac{3V_{DA}}{4\pi}} = r_{cr}\sqrt[3]{\frac{n_{cr}}{\pi}}\sqrt[6]{18}. \tag{2.34}$$

The volume ratio between n_{cr} IONC spherical volume, $V_{r_{cr}}$ and n_{cr} IONC dense aggregate volume, $V_{R_{DA}}$ influences the magnetization volume of the effective packed spherical aggregates, M_{DA}. The influence of the volume ratio on M_{DA} can be expressed using equation (2.18):

$$M_{DA} = LM_{cr}\frac{V_{r_{cr}}}{V_{R_{DA}}} = LM_{cr}\frac{n_{cr}\frac{4\pi r_{cr}^3}{3}}{n_{cr}\frac{4\pi.r_{cr}^3}{3}\frac{\sqrt{18}}{\pi}} \tag{2.35}$$

The simplified expression for equation (2.18) is:

$$M_{DA} = LM_{cr}\frac{\pi}{\sqrt{18}}. \tag{2.36}$$

The concentration of iron for isotrobic expression which is equation (2.24) can be rewrite in terms of the volum ratio as below:

$$[Fe]_{DA}^{FD} = [Fe]_{iso}^{FD}(\frac{\pi}{\sqrt{18}}), \tag{2.37}$$

where FD stands for fast diffusion. Finally by combing equations [2.33-2.37], the transverse relaxivity of dense spherical aggregates can be determined by rewriting equation (2.26) as [4]:

$$r_{2,DA}^{FD} = \frac{16}{1215}\frac{m_{Fe_3O_4}}{\rho}(\gamma\mu_0 M_{cr}L)^2\frac{r_{cr}^2}{D}\sqrt[6]{18}(\pi)^{\frac{1}{3}}n_{cr}^{\frac{2}{3}}. \tag{2.38}$$

The simplified form of equation (2.38) gives the transverse relaxivity of the dense spherical aggregate IONCs:

$$r_{2,DA}^{FD} = r_{2,FD}^{iso}\sqrt[6]{18}(\pi)^{\frac{1}{3}}n_{cr}^{\frac{2}{3}}. \tag{2.39}$$

From the theory perspective equation (2.38) shows that the proportionality of the transverse relaxivity with the number of particles in the dense aggregate [6]. Meanwhile equation (2.34) shows the relation between the radius of the aggregate and the number of particles. The aggregate size that satisfies the condition of motional average regime, since τ_D is proportional to the square of aggregate radius

then $r_{2,DA}$ increases with the aggregate size. In the motional average regime, the transverse relaxivity increase with the aggregate size and saturates in the static regime as described in [7]. In the packing aggregate, the radius of the aggregate and the number of particles in the aggregate expressed by the fractal dimension, fd as described by [2, 6, 18, 24]:

$$n_{cr} = R_{DA}^{fd}, \tag{2.40}$$

where fd is the fractal dimension, which an index for characterizing fractal patterns. For fully packed spherical aggregates fd is 3 and for loose aggregate is 2 [2, 24].

2.2.2 Static dephasing regime

When the IONCs are in the motional average regime, their effect on the relaxation time comes from the diffusion of protons of the water molecules surrounding the particles. Molecules, which interchange their position in inhomogeneous field created by the IONCs leads to the dephasing of the water protons. This phenomena is effective for a fast diffusion regime i.e. when the inverse diffusional correlation time, τ_D^{-1} is much larger than angular frequency shift experienced by water protons at the particles' equator, $\delta\omega$ [2, 4, 19].

When the condition, $\tau_D < \delta\omega^{-1}$ is not fulfilled, there is also another phenomena that affects the relaxation time, which is the case for large particles [19]. The water protons are quasistatic and this regime is called static dephasing regime. In the static regime the effect on transverse relaxation time arises from the difference in local nuclear frequencies and the difference of the frequencies results to a collection of different spin phases in the sample [19]. According to [2, 6], the transverse relaxation rate is proportional to the dephasing of the spins caused by the spread local frequencies, $\delta\omega$ and given by:

$$R_2^{SD} = af\delta\omega, \tag{2.41}$$

where a is a geometric factor and determined from the distribution function for the particle's radius, R, $P_R(R)$ and equal to $\frac{2\pi}{3\sqrt{3}}$ [19], $\delta\omega$ and f are described earlier. For a gradient echo sequence, the relaxation rate, R_2^* induced by the spherical IONCs can be expressed as below:

$$R_2^{SD} = \frac{2\pi}{3\sqrt{3}} f\gamma B_{eq}, \tag{2.42}$$

where B_{eq} and f intermes of $[Fe]$ are given by equation (2.20) and (2.24) respectively. The transverse relaxivity of IONCs in static dephasing regime is given as followed by.

$$r_2^{SD} = \frac{2\pi}{27\sqrt{3}} \frac{m_{Fe_3O_4}\gamma\mu_0 M_{cr} L}{\rho}. \tag{2.43}$$

This theory is characterized by the conditions $\tau_D > \delta\omega^{-1}$ [2, 4, 19]. This theory predicts the maximum transverse relaxivity for a given particles' volume fraction, f and spherical particles average radius if the condition introduced by Yablonskiy and Haacke fulfilled [19, 25].

For a given f,

$$r_{cr}^2 >> \frac{6D}{\delta\omega f^{\frac{1}{3}}}. \tag{2.44}$$

And for a given r_{cr},

$$f >> \frac{6D}{(r_{cr}^2\delta\omega)^3}. \tag{2.45}$$

Yablonskiy and Haacke have also noticed that the above conditions are particles' shape dependant and the expressions are given for spherical particles. In a close range the magnetic field created by the particles is sensitive to the shape of the particles [19].

2.2.3 Exchange model

This model is important in describing the transverse relaxivity when both the fast diffusion and the static dephasing regime short to predict the transverse relaxivity . The residence lifetime of protons,τ_D, plays a crucial role in determining the proton relaxivity and it has its own contribution to the characteristic time τ_D [9]. In the case of exchange protons between different systems, which each having its own specification relaxation rate, the contribution comes from the residing protons or through the exchange of the water molecule itself. According to Yves et.al., if there is a proton exchange dominancy, the transverse relaxivity is proportional to the ratio between the total number of adsorption sites for protons per litter of solution, and C_T, the concentration of solvent protons involving in the exchange and given by [26]:

$$R_2^{EX} = \frac{C_T q}{C_V}\frac{1}{T_2^M + \tau_m}, \tag{2.46}$$

where q is the number of protons adsorbed on one magnetic entity, T_2^M is the relaxation time of an adsorbed protons, τ_m is the residence time of an adsorbed proton on the magnetic entity and C_T given a bulk proton concentration. According to equation 2.46, R_2 depends on the number of protons involving in the exchange. Then the exchange model can predict, an increase relaxation rate with an increase static volume fractions. In our case the exchange model with an appropriate analytical equation and simulations can give us better understanding on the role of water protons in the PEG coating and exchange between water in PEG coating and bulk water in the r_2 of IONCs.

3 | Method

3.1 Synthesis of NEs

NEs were prepared of the phospholipids PEG2000-DSPE, DSPC and soybean oil. Two different NEs, which differ in their PEG2000-DSPE content were prepared in this thesis. They are referred to as P10 and P50, where P stands for PEG2000-DSPE and 10 and 50 represents the mol% of the added PEG2000-DSPE respectively. The components were mixed at the desired molar ratios and the desirable size of the nanoparticles was controlled by the amount of soybean oil. The molar ratio of the two phospholipids and the amount of soybean oil added to the NEs is shown in table 4.1.

Particles	DSPC(mol%)	PEG2000-DSPE (mol%)	Soybean oil(mg/μmol lipds)
P10	90	10	2.4
P50	50	50	5.41

Table 3.1: Lipid and soybean oil content of the different batches

All the required amount of lipids and soybean were prepared in separate stock solutions in chloroform with a concentration of 25 mg/ml DSPC, 25 mg/ml of PEG-DSPE and 500 mg/ml of soybean oil. The stock of iron oxide particles was prepared by the manufacturer and the concentration was 5 mg/ml. Then all the components were mixed together and added dropwise to 5 ml of 75^oC deionized water, which led to an instantaneous evaporation of the chloroform. Immediately after finishing the mixing, the crude emulsion was mixed by vortex mixer for two minutes and was cooled under tap water.

Finally the crude emulsions were maintained at room temperature and were sonicated to break down into smaller size using a thin sonicator tip for 20 minutes. Sonicator tip scraps and other residues were removed with centrifugation at 4500 rpm for 5 minutes. Some part of the procedures were supported by the following

photos, which were taken during the NEs preparation in NTNU nanolab.

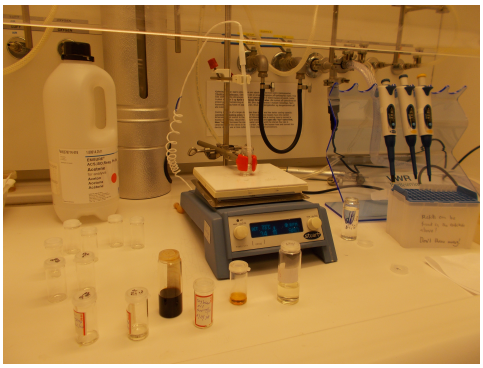

Figure 3.1: Photo taken from NEs preparation in Nanolab

Figure 3.2: Drop wise mixing

3.2 Characterization of the NEs

After NEs preparation, different characterizations were performed to confirm the necessary parameters of the NEs. A series of different measurements in different instruments were performed to obtain the experimental values of the transverse relaxivity of the IONCs.

3.2.1 Dynamic light scattering (DLS)

The hydrodynamic size and size distribution of the droplets were measured using dynamic light scattering technique (Malvern, Zetasizer Nano PS). DLS is a widely used and relatively simple technique to determine the size distribution of different particles. This technique determines the particles size by measuring the rate of diffusion of the particles through a fluid using the principles of Brownian motion and Photon Correlation Spectroscopy [27]. Particles were illuminated by laser light and the light is scattered by the diffused particles. The scattered light is recorded with a photomultiplier tube detector.

The random motion caused by the Brownian motion of the particles can create an intensity fluctuation. From this intensity fluctuation, the diffusion coefficient of the particles can be determined by Stokes-Einstein equation. Based on the Stokes-Einstein equation [27], at a given viscosity and constant temperature, the diffusion coefficient (D) of the Brownian motion of the NPs is inversely proportional to the

particles size as expressed in equation (3.1):

$$D = \frac{K_B T}{3\pi\eta d}, \tag{3.1}$$

where, K_B is Boltzmann constant (1.38×10^{-23} J/^oK), T is temperature (^oK), η is viscosity of the solution and d is equivalent spherical diameter. So by correlating the intensity fluctuation with the diffusion coefficient of the particles, we can determine the particle size and size distribution of the particles.

The DLS measurements were performed immediately after the emulsions were prepared. The emulsions were diluted to the desirable concentration before the measurement. 20 μl of NEs suspension was dispersed in 1.4 ml deionized water in a cuvette as shown in figure 3.2

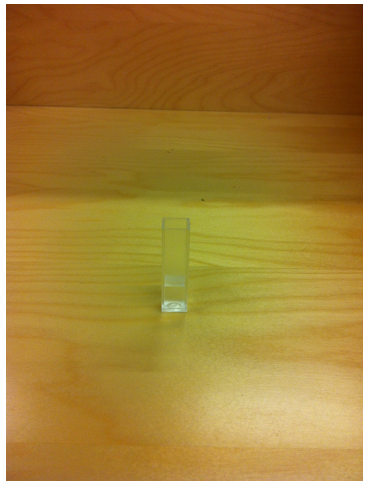

Figure 3.3: sample for DLS in Ordinary cuvette

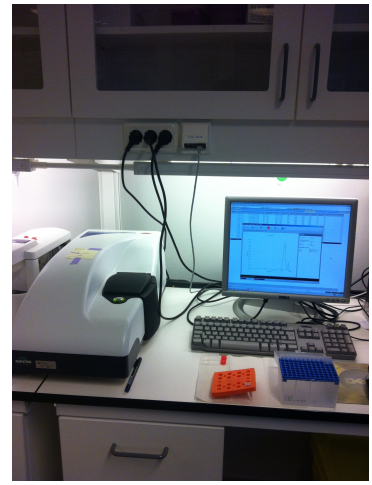

Figure 3.4: Dynamic Light Scattering (Malvern, Zetasizer Nano PS)

3.2.2 Inductively coupled plasma mass spectrometry

High resolution inductively coupled plasma mass spectrometry (ICP-MS) was performed at the department of chemistry at NTNU. 1 ml emulsion samples were diluted in 1 ml 50% nitric acid and analyzed on a ELEMENT 2 from Thermo Electronics. Then the concentrations of phospholipids and iron in the emulsion were measured using ICP-MS.

3.2.3 Transmission Electron Microscopy (TEM)

The IONC distribution in the NEs were imaged with TEM. 20 μl of emulsion was mixed with 20 μl of 2% phosphotungstic acid solution in ultrapure water. Subsequently, 20 μl of this mixture was pipetted onto a TEM grid and excess liquid was blotted away with filter paper. Samples were allowed to air dry for minimum 4 hours before imaging on the same day was performed on a Hitachi S-5500 S(T)EM.

3.2.4 Relaxivity measurements at four field strengths

In order to determine the transverse relaxivities (r_2), T_2 measurements of different samples were performed at four different field strengths. A dilution series of 4 samples of each batch with different Fe concentrations ranging from 0.05 to 1 mM were prepared. The dilution series of samples with their respective iron concentration are shown in tables 4.2 and 4.3.

	Fe concentration (mM)in the diluted samples			
Batch	sample 1	sample 2	sample 3	sample 4
1	0.03	0.015	0.0075	0.00375
2	0.072	0.036	0.018	0.009
3	0.135	0.0675	0.03375	0.0169
4	0.116	0.058	0.029	0.0145
5	0.073	0.0365	0.0183	0.009
6	0.095	0.0475	0.02375	0.0118

Table 3.2: Fe concentration in each diluted sample(P10 batches).

	Fe concentration (mM) in the diluted samples			
Batch	sample 1	sample 2	sample 3	sample 4
1	0.0156	0.0078	0.0039	0.000195
2	0.046	0.023	0.0115	0.00575
3	0.053	0.0265	0.013	0.0066
4	0.095	0.0475	0.024	0.0119
5	0.123	0.062	0.0308	0.015
6	0.1	0.05	0.025	0.0125
7	0.12	0.06	0.03	0.015

Table 3.3: Fe concentration in each diluted sample(P50 batches).

On the **Minispec(0.47T,** 40^oc**)**, T_2 measurements of the different samples were performed. As the operating temperature of the minispec was 40^oc, each sample stayed inside a 40^oc hot water for approximately 10 minutes before the measurement was started. T_2 curves were obtained using Carr-Purcell-Meiboom-Gill (CPMG) spin echo sequence with a repetition time (TR): 6-20 s, echo spacing: 0.5 ms, 1200 recorded echo's and 8 averages.

Figure 3.5: Minispec,Bruker

On the **clinical scanners(1.5 and 3 T,** 24^oc**)**, all the samples of one particle (P10 or P50) were placed in manually prepared sample holder as shown in fig 3.10. A T_2 map was obtained with a multiple spin echo sequence with 32 echoes, 15 ms echo spacing time, 4000 ms repetition time and a matrix size of 256×256. MR data was analyzed using Matlab. T_2 was determined by region of interest measurement of the samples on the T_2-map and calculated by performing fits of multiple images to a monoexponential decay.

Similarly on the **Biospec (7 T horizontal bore magnet,** 24^oc**)**, 8 samples of two batches were placed in a sample holder, of which a T_2 map was obtained with

a spin echo sequence with 64 echoes, 11.2 echo spacing time and 15 s TR. The data was analyzed in similar way as the clinical scanners.

After having T_2 of each sample in both scanners, the relaxation rate ($R_2 = 1/T_2$) was determined. The relaxation rate was plotted against the iron concentration in mM and r_2 of each batch was calculated from the slope of the respective graph according to equation (2.22).

Figure 3.6: orientation of samples before scanning

Figure 3.7: 3T scanning of the samples using body coil

4 Results

4.1 Experimentally measured properties of the different NEs.

NEs with 10 and 50 mol% of PEG2000-DSPE contents which are referred as P10 and P50 respectively were prepared using a stirring magnet mixing approach. To keep the NEs size constant, the soybean oil content was optimized and it was added in amounts expressed as mg/μmole of the amphiphillic lipids(a total of 5 μmole of amphiphillic lipids). The optimum amount of oil added was 2.4 and 5.3 mg/μ mole for P10 and P50 respectively to find the same size for all batches, which is important to exclude the size effect on the relaxivity.

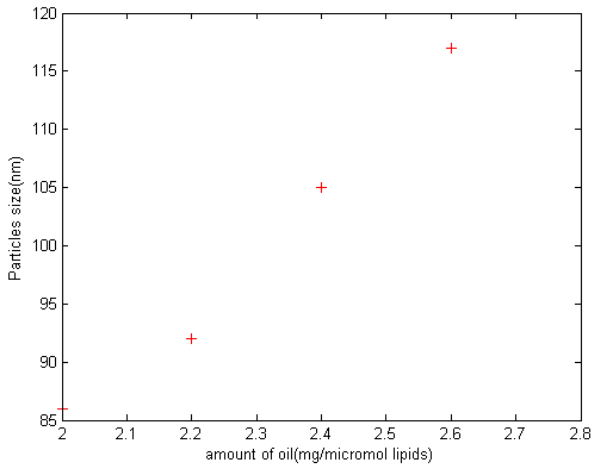

Figure 4.1: Optimum size for P10 at 2.4 mg/μ mole

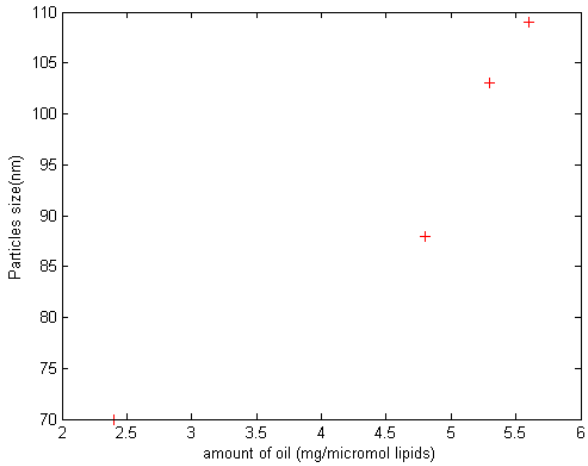

Figure 4.2: Optimum size for P50 at 5.5 mg/μ mole

From the above graph, the amount of soybean oil for P50 is higher than P10. As explained by Hak et al. [28], as the amount of the PEG2000-DSPE increased the size of the NE droplet decreased. The author explained the reason as "PEG2000-DSPE having a very low critical packing parameter ($\approx$0.05), which reflects the dimensional proportion between the hydrophobic and hydrophillic part of an amphiphile. Hence, in PEG2000-DSPE the hydrophilic polymer is very large relative to the hydrophobic fatty acid tails. This large hydrophilic polymer tends to increase the curvature of the membrane in which the lipid incorporates, decreasing the diameter of the particle." Additionally it has been observed that PEG lipids can cover (stabilize) larger surface areas at interface with increasing PEG content in the lipid layer.

4.1.1 Size, Size Distribution and Concentration of the NEs

After successful preparation of the NEs, the hydrodynamic size and the concentration of phospholipids and iron in the oil droplet were measured for both P10 and P50 NEs. The data are tabulated in table 4.2 and 4.3 respectively.

Batch	Size(nm)	PDI	[P](mM)	[Fe](mM)
1	103	0.094	0.53	0.03
2	105	0.099	0.61	0.072
3	109.5	0.269	1.03	0.27
4	109	0.175	0.62	0.35
5	108	0.148	0.59	0.73
6	95.5	0.212	0.65	0.95
Average	105			

(a)

Batch	Size(nm)	PDI	[P](mM)	[Fe](mM)
1	97	0.12	0.78	0.016
2	105	0.11	0.63	0.046
3	98	0.12	0.75	0.110
4	107	0.11	0.70	0.250
5	97	0.098	0.79	0.620
6	106	0.10	0.80	1.03
7	108	0.10	0.72	1.83
Average	102.6			

(b)

Table 4.1: The recorded concentrations were obtained from ICP-MS measurements. While the hydrodynamic diameters and polydispersity were obtained from DLS measurements. The recorded hydrodynamic diameters are the average value of three measurements and they are corresponding to the number average distribution of the DLS measurements. Where as the polydispersity index (PDI) is a measure of the size distribution broadness and obtained as the standard deviation divided by the average value. The PDI also gives an indication of monodispersity of the particles(a) for P10 and (b) for P50

We prepared NEs with well-controlled size and IONCs contents. The size of the droplet was tuned easily to obtain a similar size for all the batches. This allowed us to minimize the effect of the particles size on the relaxivity. As shown in table 4.1, the iron concentration increased as the amount of IONCs in the oil core increased while the amount of IONCs didn't affect the droplet size.

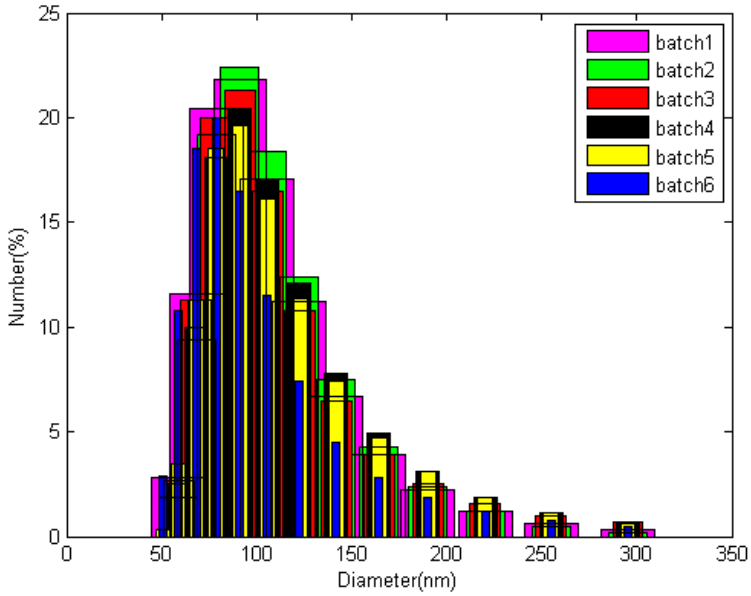

Figure 4.3: Histograms of particle size distributions (P10) provided by the size distribution processor (SDP)

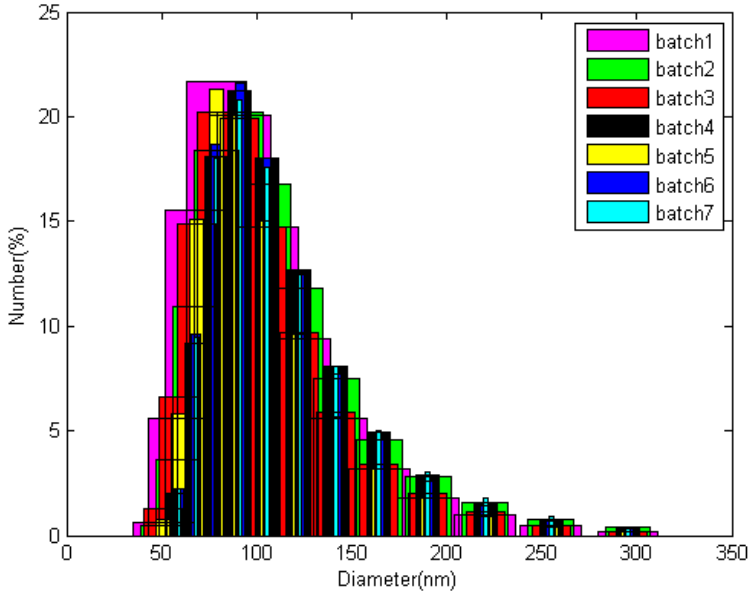

Figure 4.4: Histograms of particle size distributions (P50) provided by the size distribution processor (SDP).

TEM

In figures 4.5-4.8, a TEM images of two batches from each particle are shown. TEM images of batch 3 and batch 6 of P10, figures 4.5 and 4.6 respectively, show slightly bigger cluster size than the size measured by DLS and show an even distribution of IONCs in the NE core. Whereas in figures 4.6-4.8, a TEM images of P50 batches show the presence of larger clusters (figures: 4.7 and 4.8) and figure:4.9 shows an image of only scattered IONCs, no real cluster, just black dots throughout the image.

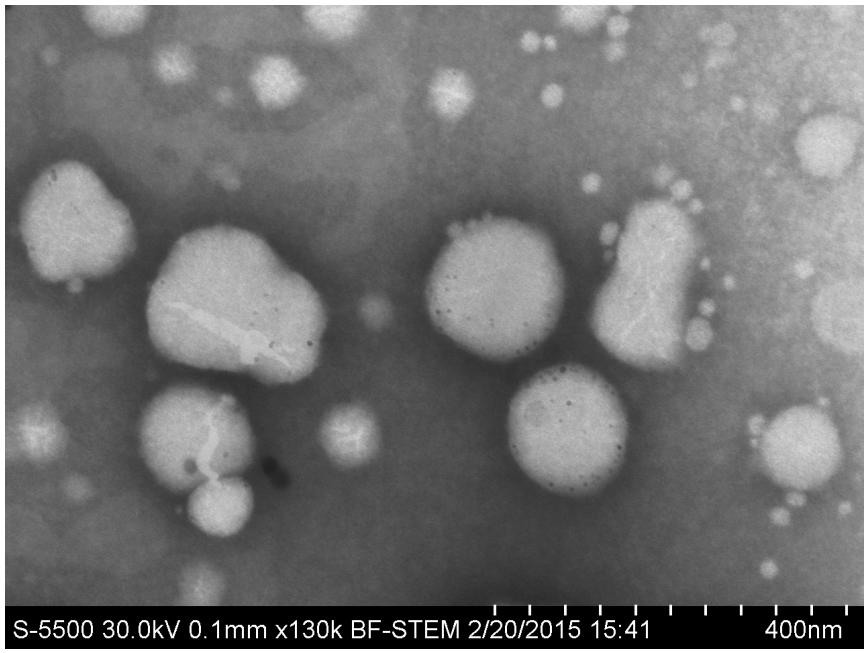

Figure 4.5: TEM image of P10 Batch 3

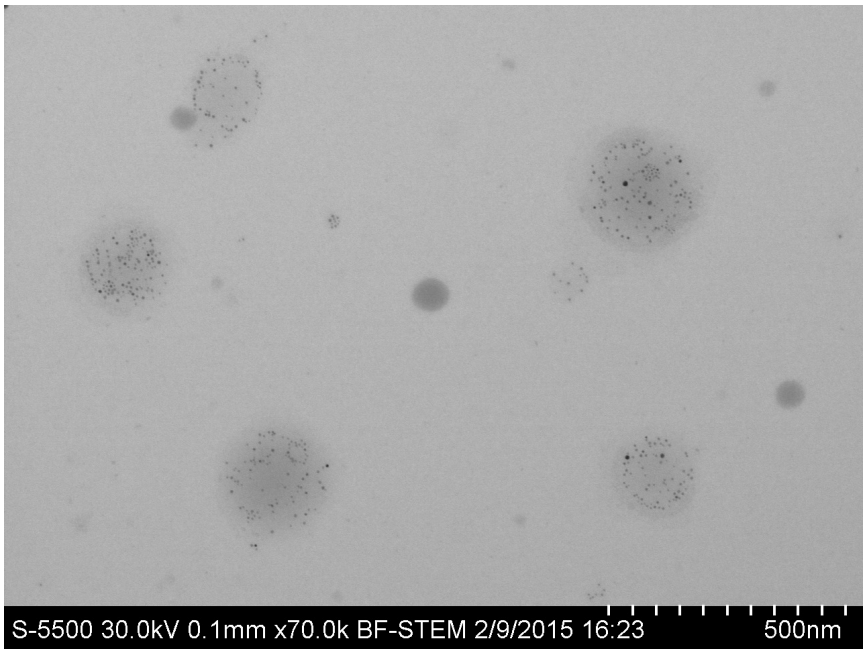

Figure 4.6: TEM image of P10 Batch 6

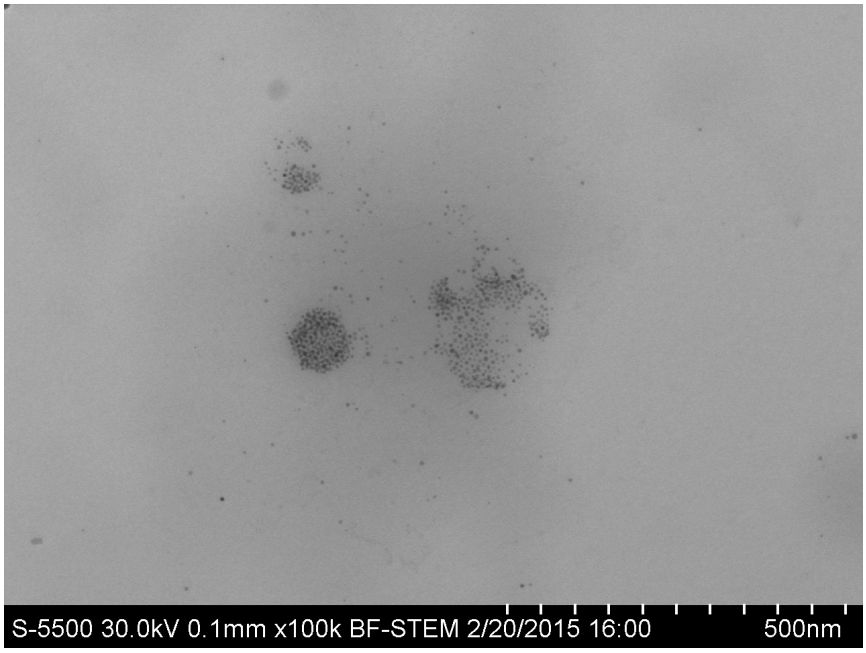

Figure 4.7: TEM image of P50 Batch 6

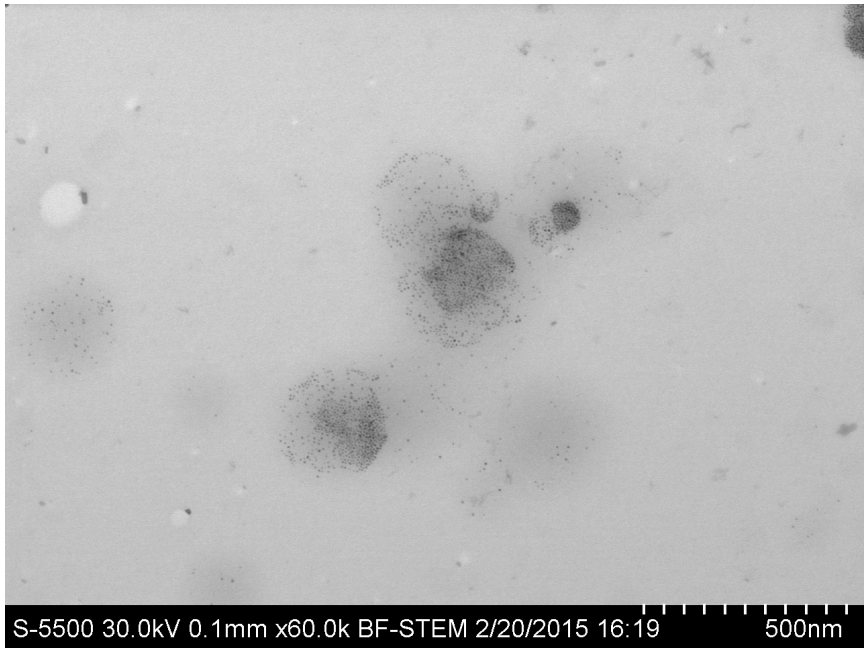

Figure 4.8: TEM image of P50 Batch 7

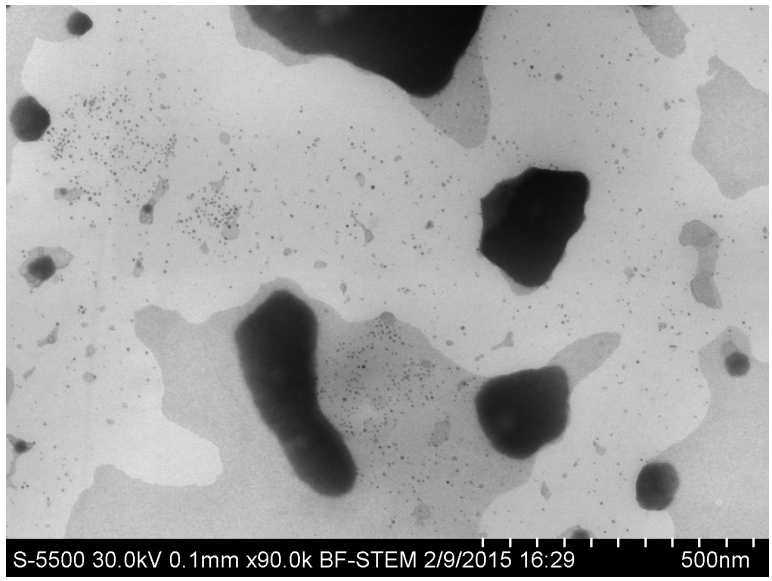

Figure 4.9: Scattered IONCs overall in the NE

4.1.2 Experimental Transverse Relaxivity (r_2) of the different NEs

Transverse relaxivities were measured at Minispec, Bruker (0.47T (40^oC)), at clinical scanners (1.5T and 3T(24^oC)) and at Biospec, Bruker (7 T and 24^oC). T_2 of each sample at the Minispec was determined using a CPMG spin echo sequence protocol: While On the other scanners the T_2 map was obtained with a multiple spin echo sequence. The T_2 maps for the clinical scanner and biospec are shown in figure 4.10 and figure 4.11 respectively. The corresponding experimental relaxivities of the different batches of P10 and P50 are shown in table 4.2 and 4.3 respectively. The values of R^2 indicates the goodness of fit of the graph. It measures the proportion of the variation of the observations around the mean that is described by the fitted regression model [29]. The closer R^2 is to 1, the greater the degree of association between relaxation rate and iron concentration.

The transverse relaxivities of the different batches at different magnetic field strength also plotted as shown in figure 4.12 and 4.13

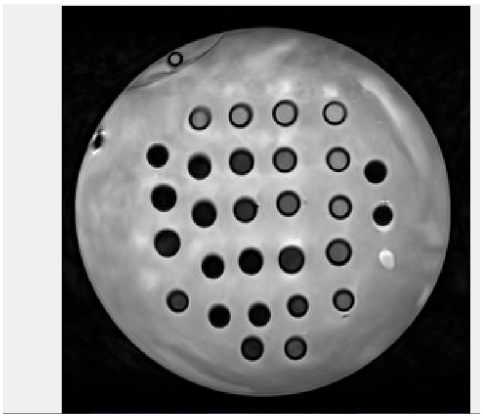

Figure 4.10: T2−map of 28 samples obtained from 1.5 T scanner

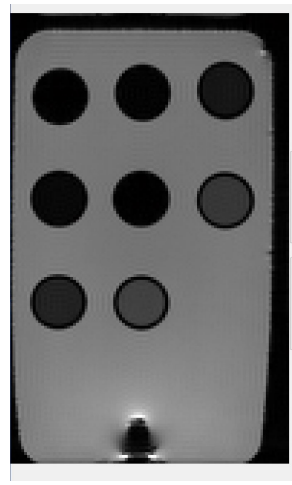

Figure 4.11: T2−map of 8 samples obtained from 7 T scanner

Batch	0.47 T	(R^2)	1.5 T	(R^2)	3 T	(R^2)	7 T	(R^2)
1	27	0.99	56	0.98	59	0.98	52	0.98
2	28	0.98	62	0.95	62	0.94	68	0.93
3	51	0.99	119	0.99	108	0.99	110	0.99
4	60	0.99	152	0.99	142	0.99	155	0.99
5	63	0.99	194	0.99	180	0.99	191	0.99
6	91	0.99	248	0.99	226	0.99	252	1.00

Table 4.2: Experimental relaxivities ($mM^{-1}s^{-1}$)of the different P10 batches.

Batch	0.47 T	(R^2)	1.5 T	(R^2)	3 T	(R^2)	7 T	(R^2)
1	98	0.99	179	0.99	162	0.99	242	0.99
2	132	0.98	259	0.99	223	0.97	308	0.98
3	126	0.99	247	0.99	203	0.99	292	0.99
4	139	0.99	262	0.99	195	0.96	317	0.99
5	102	0.99	197	0.99	185	0.99	248	1.00
6	157	0.99	281	0.99	202	0.98	335	0.99
7	176	0.99	308	0.99	265	0.99	369	1.00

Table 4.3: Experimental relaxivities ($mM^{-1}s^{-1}$) of the different P50 batches.

4.2 Estimation of IONC content of the different NEs

From the TEM image of the NEs, we saw clustered IONCs for P10 (figures: 4.5 and 4.6) and unevenly dispersed IONCs for P50 (figure: 4.9). The effect of clustering of IONCs on the relaxivities was examined by plotting the transverse relaxivities as a function of the number of IONCS in the oil droplet. So using the above experimentally obtained properties, the amount of IONCs in the oil core of each batches were calculated. The quantification of iron and phosphorus from the ICP measurement was used to estimate the number of IONCs in the NE droplets. The volume and surface area of oil per droplet are calculated from PEG layer deducted hydrodynamic radius (r_{dr}). The hydrodynamic radius of the spherical droplet shape is obtained from the DLS measurement (table 4.1 a and b). However the thickness of the PEG layer for each particles of P10 and P50 was calculated by using equation (2.28) with the number of monomers per chain ($N = 45$ for PEG2000) and the length of a monomer a=0.35 nm [30]. The distance between the anchoring points of the PEG chain, D for P10 and P50 was also calculated from the molar percentages of each lipid present in the different NEs and the surface area of DSPC and DSPE (0.64 nm^2 and 0.72 nm^2 respectively) [31]. For P10, the NE has a molar ratio PEG2000-DSPE:DSPC equal to 1:9 and according to [31], it can be assumed that one PEG chain covers 6.48 nm^2. Similarly P50 with molar ratio of 1:1, one PEG chain covers 1.36 nm^2. If the surface area covered by one PEG chain is assumed to be a circle then D equals the diameter of it [28], which means that the distance between the anchoring points of the PEG chain for P10 and P50 is equal to 2.87 nm and 1.32 nm respectively. Finally, according to equation (2.28),

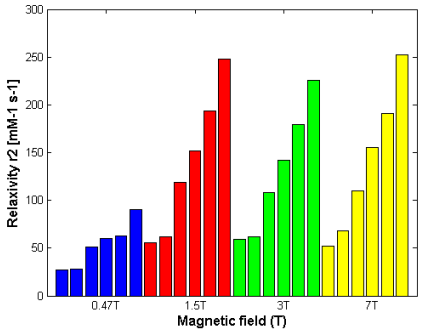

Figure 4.12: r2 of P10 batches plotted at different magnetic field

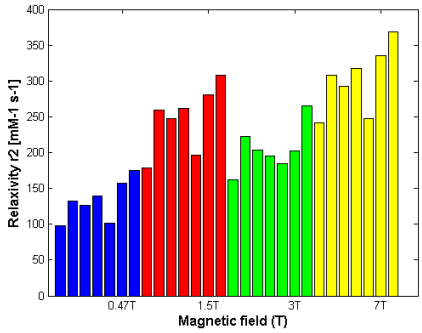

Figure 4.13: r2 of P50 batches plotted at different magnetic field

one can calculate the thickness of PEG layer for P10 and P50, taking into account that the NE is spherical, the distance between PEG chains is increased at the outer surface, the thickens is 3.77 nm and 6.2 nm respectively.

Therefore the volume and the surface area of oil per droplet are determined as $V_{dr} = 4/3\pi(r-l_{PEG})^3$ and $A_{dr} = 4\pi(r-l_{PEG})^2$ respectively. Now the number of phospholipids per droplet can be calculated from the surface area of the droplets and the average surface area per lipid, which is 0.68 [4]. From the number of phospholipids per droplet and the phosphorus concentration, which is one phosphor atom per one phospholipid, the droplet concentration is obtained. Iron concentration in the oil was calculated from the iron concentration and the droplet concentration, which in turn helps to estimate the number of μmoles of iron per droplet.

The final out put of all the above estimations were to find the number of IONCs inside each droplet and estimated from the following simple calculation. Given that the density and molar mass of 5 nm IONCs consisting of Fe_3O_4 5.1g/cm^3 and 231.5g/mol respectively [4], the number of mole of iron that one IONC contains can be estimated from the molar volume of Fe_3O_4 and volume of one IONC:

$$V_{molar} = \frac{231.5\frac{g}{mol}}{5.1\frac{g}{cm^3}}. = 45.4\frac{cm^3}{mol} \tag{4.1}$$

Since Fe_3O_4 contains 3 Fe atoms the molar volume of Fe is 15.1 cm^3/mole (45.4/3). The volume of a single 5nm IONC is:

$$V_{IONC} = \frac{4}{3}\pi(2.5)^3 = 6.5 \times 10^{-20} cm^3. \tag{4.2}$$

Now by combining equation (4.1) and 4.2, the number of moles Fe in 1 IONC is calculated as:$(6.5/15.1)\times10^{-20}$=4.3×10^{-21}mole. Finally, the mean number of IONCs per NE droplet is estimated based on the number of μmoles of iron per

droplet and the number of moles in 1 IONC (4.3×10^{-21}mole). The estimated values are listed in the tables 4.4 and 4.5. Similarly the Estimated amount of

Batch	Volume of oil per droplet (cm^3) $\times10^{-16}$	Surface area per droplet (cm^2) $\times10^{-10}$	nr of lipids per droplet $\times10^4$	[droplet] (mM) $\times10^{-5}$	[Fe] in oil core (mM)	μmoles Fe per NE droplet $\times10^{-21}$	nr of IONCs perNE droplet
1	4.55	2.86	4.21	1.26	8.69	3.96	0.916
2	4.85	2.98	4.39	1.39	17.7	8.6	1.99
3	5.55	3.27	4.8	2.14	37.7	20.9	4.84
4	4.47	3.23	4.76	1.30	81.5	44.6	10.3
5	5.30	3.17	4.66	1.27	179	95.1	22.0
6	3.56	2.43	3.57	1.82	243	86.8	20.1

Table 4.4: Estimated amount of IONC at different p10 batches.

IONCs for different P50 batches also shown on *table*4.7

Batch	Volume of oil per droplet (cm^3) $\times10^{-16}$	Surface area per droplet (cm^2) $\times10^{-10}$	nr of lipids per droplet $\times10^4$	[droplet] (mM) $\times10^{-5}$	[Fe] in oil core (mM)	μmoles Fe per NE droplet $\times10^{-21}$	nr of IONCs perNE droplet
1	3.17	2.25	3.30	2.36	3.47	1.1	0.25
2	4.16	2.69	3.96	1.6	11.5	4.77	1.1
3	3.28	2.30	3.39	2.21	24.4	8	1.85
4	4.43	2.81	4.13	1.69	63	27.9	6.47
5	3.17	2.25	3.30	2.40	134	42.6	9.87
6	4.29	2.75	4.04	1.99	199	85.3	19.76
7	4.57	2.78	4.22	1.69	390	179	41.33

Table 4.5: Estimated amount of IONC at different p50 batches.

After having all the estimated values, the transverse relaxivities of the different batches were plotted as a function of the estimated IONCs per droplet and indicated in figure 4.14 and 4.15.

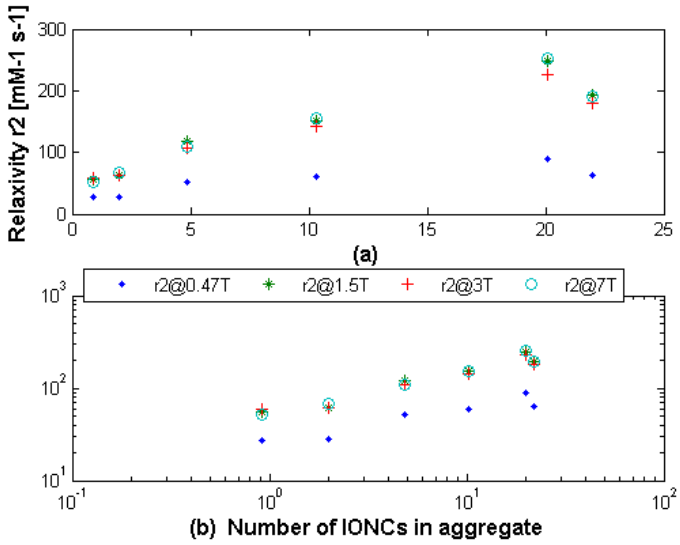

Figure 4.14: a) plot of relaxivities for P10 as a function of mean number of IONCs in the NEs at different magnetic field. b) loglog plot of figure a)

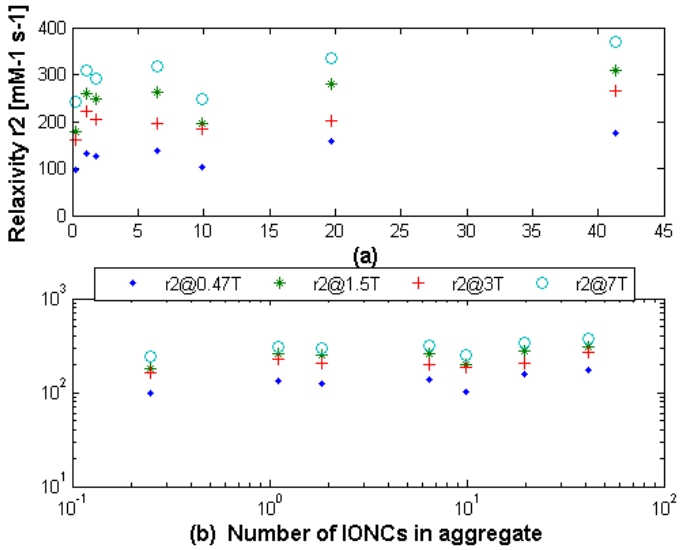

Figure 4.15: a) plot of relaxivities for P50 as a function of mean number of IONCs in the NEs at different magnetic field. b) loglog plot of figure a)

4.3 Model fitting

Experimental results were fitted with the theoretical models in Matlab. The transverse relaxivities as predicted by all four different theoretical models were calculated. The prediction included the NE polydispersity for the dense and loose aggregate model and the corresponding values at different magnetic fields are tabulated in 4.6 and 4.7.

	Isotropic				Loose Aggregate				Dense Aggregate				Static Dephasing			
Batch	0.47T	1.5T	3T	7T	0.47T	1.5T	3T	7T	0.47T	1.5T	3T	7T	0.47T	1.5T	3T	7T
1	1.1	5.0	6.4	7.3	0.8	0.4	0.5	0.5	1.5	6.6	8.4	9.4	185	341	383	407
2	1.1	5.0	6.4	7.3	0.2	0.7	0.9	1.1	2.3	10	13	15	185	341	383	407
3	1.1	5.0	6.4	7.3	0.5	2.0	2.6	2.9	4.9	22	28	32	185	341	383	407
4	1.1	5.0	6.4	7.3	1.0	4.3	5.5	6.2	8.2	37	46	52	185	341	383	407
5	1.1	5.0	6.4	7.3	2.1	9.5	12	13	14	62	78	88	185	341	383	407
6	1.1	5.0	6.4	7.3	2.5	11	14	16	15	66	83	94	185	341	383	407

Table 4.6: Theoretical model predictions for r_2 of the different P10 batches.

	Isotropic				Loose Aggregate				Dense Aggregate				Static Dephasing			
Batch	0.47T	1.5T	3T	7T	0.47T	1.5T	3T	7T	0.47T	1.5T	3T	7T	0.47T	1.5T	3T	7T
1	1.1	5.0	6.4	7.3	0.02	0.1	0.1	0.1	0.6	2.6	3.3	3.7	185	341	383	407
2	1.1	5.0	6.4	7.3	0.1	0.4	0.5	0.6	1.6	7.1	9.0	10	185	341	383	407
3	1.1	5.0	6.4	7.3	0.2	0.7	0.9	1.0	2.2	10	12	14	185	341	383	407
4	1.1	5.0	6.4	7.3	0.5	2.3	2.9	3.3	5.0	22	28	32	185	341	383	407
5	1.1	5.0	6.4	7.3	0.9	3.9	4.9	5.6	6.6	29	37	42	185	341	383	407
6	1.1	5.0	6.4	7.3	1.6	7.0	8.9	10	10	46	59	66	185	341	383	407
7	1.1	5.0	6.4	7.3	3.4	15	19	21	18	78	99	112	185	341	383	407

Table 4.7: Theoretical model predictions for r_2 of the different P50 batches.

The analytical r_2 value for all four different theoretical models together with the experimental r_2 are plotted in Matlab and shown in the figures 4.16 and 4.17.

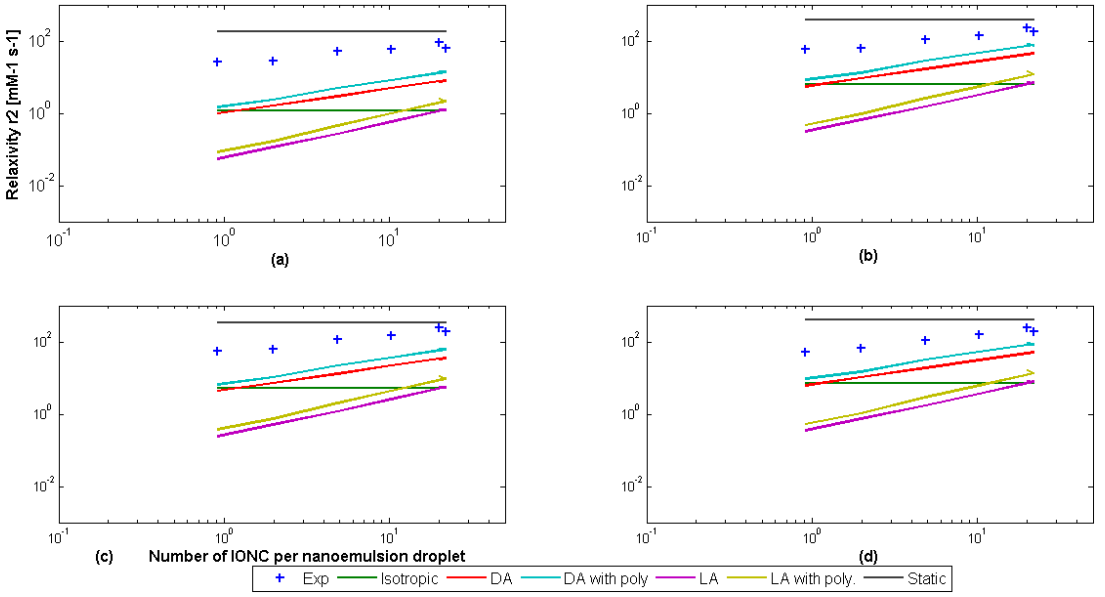

Figure 4.16: Experimental and analytical r_2 for P10 NEs,(a) at 0.47T, (b) at 3T, (c) at 1.5T and (d) at 7T

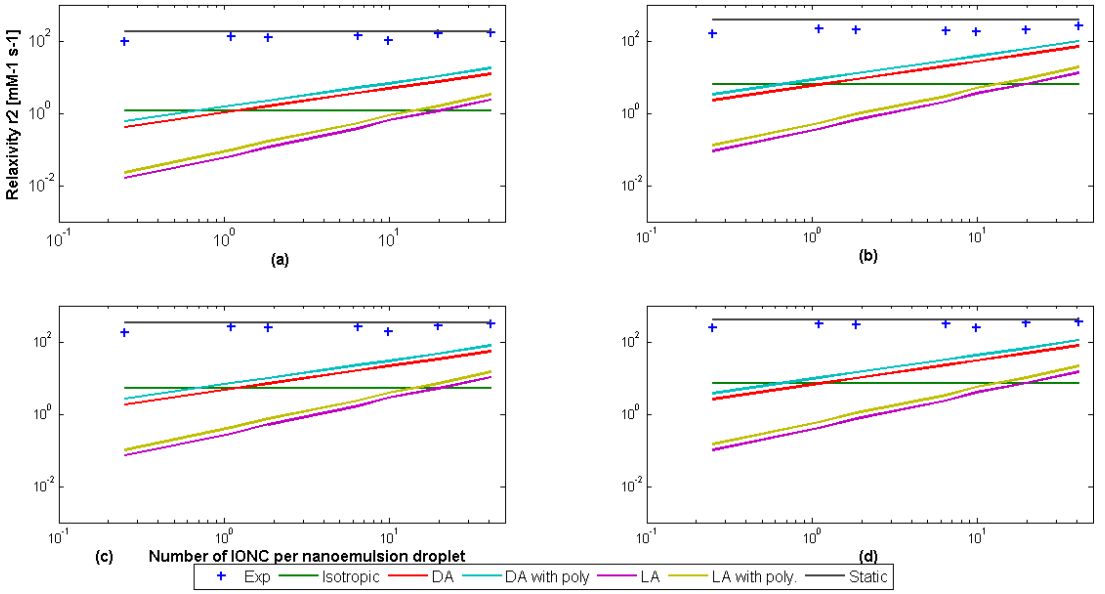

Figure 4.17: Experimental and analytical r_2 for P50 NEs,(a) at 0.47T, (b) at 3T, (c) at 1.5T and (d) at 7T

5 Discussion

A lot of theoretical and experimental studies demonstrate that magnetization and clustering of IONCs are key factors that influence their transverse relaxivity. Hak and his coauthors compared experimental transverse relaxivities of IONCs based contrast agents with different theoretical model predictions. They successfully prepared IONC clusters in NEs containing 50 mol% PEG2000-DSPE (P50) and the transverse relaxivities were measured at 0.47T and 7T field strengths. The measured relaxivities were plotted as a function of the number of IONCs in the NEs and the result showed that the relaxivities increased as the number of IONCs increased [4]. The study also reported that the experimental results were between fast diffusion and static dephasing model prediction values. The study hypothesized, the water protons entrapped in the PEG layer are the main contributors for the static dephasing regime [4].

This master thesis is the continuation of Hak's study. NEs with different PEG content and varying amounts of IONC were made. Experimental transverse relaxivities of IONCs clustered in NEs were measured at four different field strengths. The measured relaxivities were interpreted based on two parameters: the number of IONCs in each droplet and the magnetic field strength. These experimental results were compared with predicted transverse relaxivities using four different models. In addition, the effect of the PEG coating (P10 and P50) on the relaxivity was also discussed.

5.1 P50

Particles in the current study were prepared in a similar way as in the previous study [4]. The iron oxide stock was the main difference in the preparation process. The stock for the previous study was prepared in the lab with a specific amount of oleic acid, while the current study used a ready made iron oxide stock provided by the seller company with unknown amount of oleic acid.

5.1.1 DLS versus TEM measurements

The hydrodynamic size of the particles were measured by DLS and the average size was 103 nm. However, the TEM images of P50 batches (figures: 4.7, 4.8 and 4.9) show unevenly dispersed IONCs. Furthermore, the TEM images indicate the presence of much larger clusters (estimated around 250 nm) than the size measured by DLS as shown in figures 5.1 and 5.2. We also saw for the P50 was images of only scattered IONCs, no real cluster, just black dots throughout the image as shown in figure 4.9. We do not have an explanation for this discrepancy between the DLS and TEM results, but they might indicate that the P50 particles are not stable, given the fact that there was several weeks' long delay between DLS and TEM measurements. Furthermore, it illustrates that thorough characterization of these emulsions is needed in order to assure NE geometry.

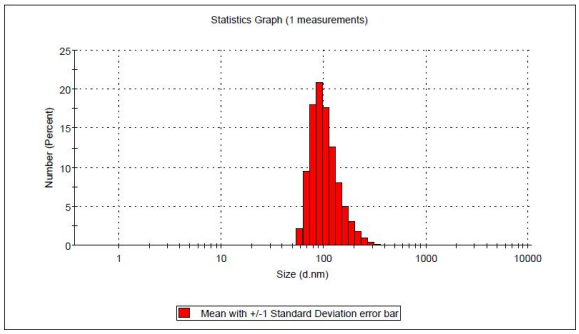

Figure 5.1: DLS size distributions of P50, batch 7

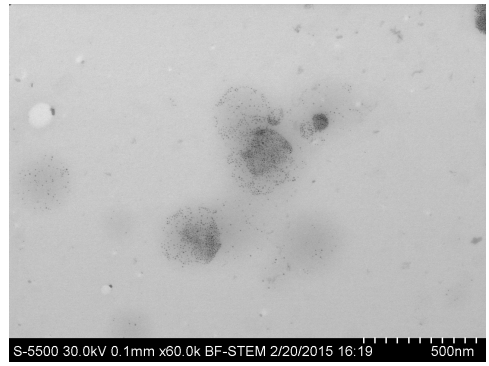

Figure 5.2: TEM image of P50, batch 7

5.1.2 Transverse relaxivities

The experimental relaxivities for the P50 particles (figures 4.15 and 4.17) do not increase as a function of the number of IONCs, in contrast to what was found by Hak et.al [4]. Additionally, the measured relaxivities were close to the prediction of the static dephasing regime model and much higher than the fast diffusion model predictions as shown in figure 4.17. Here one can understand that the diffusional regime of the bulk water can not describe this high experimental relaxivities, and one must conclude that the relaxivity is dominated by static dephasing contributions.

It is known that as the cluster size and magnetization increases, the dephasing effects are no longer correctly described by the fast diffusion model, but better described by a static dephasing model [5]. If the TEM images (and not DLS) of the

current work give the most correct description of the NE size and degree of IONC clustering, the relaxivities of P50 particles are in agreement with Poselt and his coworkers. Various studies also reported that PEG coatings have significant effects on relaxivities, although the analytical interpretation remains unclear [4, 5, 32]. A possible explanation for the static dephasing regime may result from the water in the PEG layer that could reduce water diffusivity as hypothesized in several papers [4, 5]. Based on the above considerations, there is an agreement between the analytical and experimental values. However, the current experimental results differ significantly from the previous experimental results [4]. The relaxivities in this thesis were higher and did not depend on the nr of IONC per cluster. Even though the coating type (PEG-2000) and the size (DLS) were the same, the amount of the oleic acid may cause the difference. TEM showed large aggregates in the current study, which could be the result of an excess of the amphiphilic oleic acid, which may have affected the phospholipid monolayer [33]. Overall our conclusion is that the P50 particles prepared in the current study are different than the P50 particles of our previous study in terms of size and clustering as well as the measured relaxivities. The current P50 particles seem to be larger and in the static dephasing regime.

5.2 P10

An oil-in-water emulsion method was used to develop monodisperse aggregates with an average diameter of around 105 nm. As it can be seen in the TEM images (figures 4.5 and 4.6), well-defined clusters were prepared as expected and the experimental results indicate that the higher IONCs density lead to an increase transverse relaxivities, which is similar with the previous study [4]. This is also examined using the TEM images and suggested that the clustering increased as the number of IONCs increased (4.5 and 4.6), which led to increase the relaxivity.

5.2.1 DLS versus TEM measurements

The hydrodynamic size of the particles were measured by DLS and the average size was 105 nm. TEM images are also used to confirm the cluster sizes and the distribution of the IONCs in the NE core. As shown in figures 5.3 and 5.4, some discrepancies between the two measurements are observed. The TEM image of the clusters appeared slightly distorted in shape and slightly bigger in diameter than the hydrodynamic diameter measured by DLS. The clusters may tend to collapse during TEM sample preparation, which may result in these discrepancies. But even with these discrepancies, the TEM images of P10 batches are consistent with DLS results compared to the P50 batches.

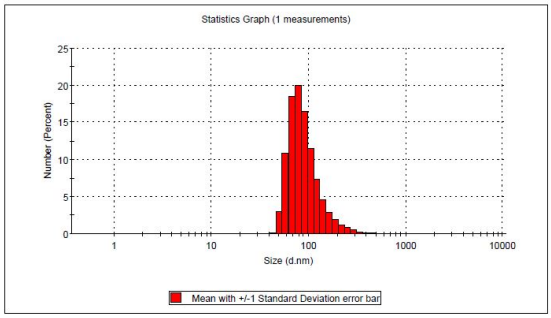

Figure 5.3: DLS size distributions of P10, batch 6

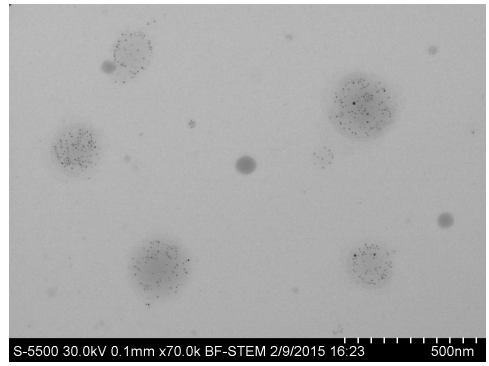

Figure 5.4: TEM image of P10, batch 6

5.2.2 Transverse relaxivities

IONC possess higher relaxivities than a uniformly distributed IONCs [34]. In this work the TEM images of the P10 batches confirmed the presence of clusters consisting of several IONCs. The TEM images of the IONCs in the batches are shown with increasing degree of clustering as indicated in figures 4.5 (batch 3) and 4.6 (batch 6, the highest number of IONCs). As shown in figure 4.14, the relaxivities also increased with increased number of IONCs in each droplet, which is in good agreement with the theoretical studies of Vuong et al. This is clearly shown in figure 4.16, the experimental relaxivities and the relaxivities predicted by dense aggregate model are increased with the number of IONCs and the loose aggregate also predicted an increase in relaxivities with the number of IONCs.

The experimental transverse relaxivities, figure 4.15 shows that the measured relaxivities are between the fast diffusion and static dephasing regime. As in equations 2.26 and 2.43 indicated, the analytical relaxivity of the fast diffusion (isotropic) and the static dephasing did not depend on the number of IONCs in the NE.

The ratio of the analytical relaxivities at two fields (0.47T and 1.5T) and at constant number of IONCs is around 4.54 for the fast diffusion models, and 1.85 for the static dephasing model. While the ratio of the experimental transverse relaxivities at 0.47T and 1.5T is around 2.75, which indicates that the experimental relaxivities are approaching to the predictions of the static dephasing regime model. This can tell us the fast diffusion regime alone can not describe the relaxivities of such NEs.

5.2.3 Effect of Polyethylene glycol (PEG) on transverse relaxivities

Even with its insufficient analytical interpretation, various studies have indicated that PEG coatings have major effects on relaxivities [32,35,36]. Tong and coworkers showed that the effect PEG coating has on the relaxivity of superparamagnetic iron oxides (SPIOs) depends both on the SPIO diameter as well as on the PEG size used in their study. They measured the transverse relaxivity with two core sizes (5 and 14 nm) and five PEG chain lengths (with molecular weights of 550, 750, 1000, 2000, and 5000). According to their observation the transverse relaxivity of the SPIOs with 14 nm size increased by 2.54-fold when the PEG molecular weight decreased from 5000 to 1000 [35]. Paquet and coworkers have also proved that the transverse relaxivity of clusters of iron oxide nanoparticles coated with in ph-responsive hydrogel increased by 85% compared to non coated clusters [32]. The authors have claimed the lower diffusivity of water inside the coating and near the particle surface for the enhancement.

In the current work it is evident that there is a significant difference in the experimental relaxivities of P10 and P50 batches. However, due to the difference in geometry between P10 and P50 we are not able to make conclusions about the effect of PEG density.

5.2.4 Magnetic field effect on the transverse relaxivities

The measured relaxivities increased with the increasing field strength. The measured relaxivities at 1.5T were around two times the relaxivities at 0.47T. However, the values of the relaxivities at 1.5T, 3T and 7T were almost the same. This is in agreement with the studies conducted by Bulte and Gossuin with their respective coathors. They have explained the effect of the magnetic field on the relaxivities and their studies demonstrate the sharp increment of transverse relaxivity with increasing magnetic field until they level of when magnetization saturation has been attained [37, 38]. According to Bulte and his coauthors all magnetite samples exhibit a T2 shortening that becomes independent of field above 0.58T due to the magnetic saturation of the cores.

5.2.5 Polydispersity

Hak and his coauthors included the effect of NE polydispersities in their modeling [4]. Previous studies of Vuong et al. and Poselt et al. discussed the effect of geometry and polydispersity on the model predictions [5, 6]. Specifically Vuong et al. has pointed towards the sample size polydispersity for the deviation between

their experimental relaxivities and model predictions. In the current work the NE polydispersity was measured and taken into account in the loose and dense aggregate fast diffusion models using a probability density function [4] as:

$$r_{2,eff} = \int_0^\infty r_2(R) pdf(R) dR, \tag{5.1}$$

where R is the radius of the NE and pdf is the probability density function corresponding to the size distribution from DLS. $r_{2,eff}$ is relaxivity where polydispersity was taken into account and calculated using Matlab. As a result fig 4.16 shows the relaxivities with and without taking polydispersity into account for the Different NE Batches. The calculated relaxivities where polydispersity taken into account increase around 40-60% compared to the relaxivities without polydispersity.

Summary and Conclusion

In conclusion, NEs with different PEG surface density (P10 and P50) and varying amounts of IONC were made. The NEs were analyzed by DLS to obtain the hydrodynamic diameter, ICP-MS to measure iron concentration, and TEM to observe the IONCs in the NEs. The experimental transverse relaxivities of IONCs clustered in NEs were measured at four different field strengths (0.47 T, 1.5 T, 3 T and 7 T).

The measured relaxivities were interpreted based on two parameters: the number of IONCs in each droplet and the magnetic field strengths.

P10:

- ☞ All experimental observations were in agreement (TEM and DLS).
- ☞ Experimental and theory was in agreement.
- ☞ Experimental relaxivities increased with increased number of IONCs in each droplet, which is in good agreement with the theoretical studies.
- ☞ Transverse relaxivities increased with increased magnetic field until they level of when magnetization saturation has been attained.
- ☞ Experimental relaxivities are between the fast diffusion and static dephasing regime.
- ☞ The ratio of experimental relaxivities was much closer to the static regime. This indicated that the fast diffusion regime alone is not appropriately describing relaxivities of the NEs.

P50:

- ☞ TEM and DLS did not agree.

- ☞ TEM agreed with the experimental relaxivities.
- ☞ TEM and relaxivities agreed with theory
- ☞ Experimental relaxivities do not increase as a function of the number of IONCs, in contrast to what was found by Hak et.al [4].
- ☞ The experimental relaxivities were close to the prediction of the static dephasing regime model and much higher than the fast diffusion model predictions.

We aimed to study the effects of PEG coating. However, The P10 and P50 are different geometry. P50 needed thorough characterization in order to assure the desired NE geometry. Therefor, it is difficult to explain what the effect of PEG coating is.

But as we have managed to make IONCs loaded NEs of a constant size, but varying PEG surface density, the effect of PEG coating for NEs with the same geometry is likely to explain by the exchange model. Further study with a thorough preparation and characterization of NEs and numerical simulations may help to understand the role of water protons entrapped in the PEG coating and proton exchange in transverse relaxivity of IONCs.

Bibliography

[1] Brooks Rodney A, Moiny Francis, and Gillis Pierre. On t2 shortening by weakly magnetized particles: The chemical exchange model. *Magnetic Resonance in Medicine*, 45(6):1014–1020, 2001.

[2] Strijkers GJ and Nicolay K. Relaxivity of nanoparticles for magnetic resonance imaging. *Handbook of Nanophysics: Nanomedicine and Nanorobotics. CRC Press: Boca Raton*, pages 1–23, 2011.

[3] Gustav J Strijkers, M Mulder, J Willem, F van Tilborg, A Geralda, and Klaas Nicolay. Mri contrast agents: current status and future perspectives. *Anti-Cancer Agents in Medicinal Chemistry (Formerly Current Medicinal Chemistry-Anti-Cancer Agents)*, 7(3):291–305, 2007.

[4] Hak Sjoerd, Goa Pål Erik, Stenmark Sebastian, Bjerkholt Frøydis F, and Haraldseth Olav. Transverse relaxivity of iron oxide nanocrystals clustered in nanoemulsions: Experiment and theory. *Magnetic Resonance in Medicine*, 2014.

[5] Poselt Elmar, Kloust Hauke, Tromsdorf Ulrich, Janschel Marcus, Hahn Christoph, Maßlo Christoph, and Weller Horst. Relaxivity optimization of a pegylated iron-oxide-based negative magnetic resonance contrast agent for t 2-weighted spin-echo imaging. *Acs Nano*, 6(2):1619–1624, 2012.

[6] Vuong Quoc Lam, Gillis Pierre, and Gossuin Yves. Monte carlo simulation and theory of proton nmr transverse relaxation induced by aggregation of magnetic particles used as mri contrast agents. *Journal of Magnetic Resonance*, 212(1):139–148, 2011.

[7] Roch Alain, Gossuin Yves, Muller Robert N, and Gillis Pierre. Superparamagnetic colloid suspensions: water magnetic relaxation and clustering. *Journal of Magnetism and Magnetic Materials*, 293(1):532–539, 2005.

[8] Peter A Jarzyna, Torjus Skajaa, Anita Gianella, David P Cormode, Daniel D Samber, Stephen D Dickson, Wei Chen, Arjan W Griffioen, Zahi A Fayad,

and Willem JM Mulder. Iron oxide core oil-in-water emulsions as a multifunctional nanoparticle platform for tumor targeting and imaging. *Biomaterials*, 30(36):6947–6954, 2009.

[9] Merbach André E and Tóth Éva. *The chemistry of contrast agents in medical magnetic resonance imaging*. Wiley Online Library.

[10] Robert W Brown, Y-C Norman Cheng, E Mark Haacke, Michael R Thompson, and Ramesh Venkatesan. *Magnetic resonance imaging: physical principles and sequence design*. John Wiley & Sons, 2014.

[11] Flower Maggie A. *Webb's physics of medical imaging*. CRC Press.

[12] Claire Corot, Philippe Robert, Jean-Marc Idée, and Marc Port. Recent advances in iron oxide nanocrystal technology for medical imaging. *Advanced drug delivery reviews*, 58(14):1471–1504, 2006.

[13] S Tamilvanan. Oil-in-water lipid emulsions: implications for parenteral and ocular delivering systems. *Progress in lipid research*, 43(6):489–533, 2004.

[14] Conxita Solans, P Izquierdo, J Nolla, N Azemar, and MJ Garcia-Celma. Nanoemulsions. *Current Opinion in Colloid & Interface Science*, 10(3):102–110, 2005.

[15] Ajay Kumar Gupta and Mona Gupta. Synthesis and surface engineering of iron oxide nanoparticles for biomedical applications. *Biomaterials*, 26(18):3995–4021, 2005.

[16] Alain Roch, Robert N Muller, and Pierre Gillis. Theory of proton relaxation induced by superparamagnetic particles. *The Journal of chemical physics*, 110(11):5403–5411, 1999.

[17] Gillis Pierre and Koenig Seymour H. Transverse relaxation of solvent protons induced by magnetized spheres: application to ferritin, erythrocytes, and magnetite. *Magnetic Resonance in Medicine*, 5(4):323–345, 1987.

[18] Matsumoto Yuri and Jasanoff Alan. T2 relaxation induced by clusters of superparamagnetic nanoparticles: Monte carlo simulations. *Magnetic resonance imaging*, 26(7):994–998, 2008.

[19] Yablonskiy Dmitriy A and Haacke E Mark. Theory of nmr signal behavior in magnetically inhomogeneous tissues: the static dephasing regime. *Magnetic Resonance in Medicine*, 32(6):749–763, 1994.

[20] Chen D-X, Sun N, Huang Z-J, Cheng C-M, Xu H, and Gu H-C. Experimental study on t 2 relaxation time of protons in water suspensions of iron-oxide nanoparticles: Effects of polymer coating thickness and over-low 1/t2. *Journal of Magnetism and Magnetic Materials*, 322(5):548–556, 2010.

[21] Cowan Brian. *Nuclear magnetic resonance and relaxation*. Cambridge University Press.

[22] Vuong Quoc L, Berret Jean-François, Fresnais Jérôme, Gossuin Yves, and Sandre Olivier. A universal scaling law to predict the efficiency of magnetic nanoparticles as mri t2-contrast agents. *Advanced healthcare materials*, 1(4):502–512, 2012.

[23] Hales Thomas C. A proof of the kepler conjecture. *Annals of mathematics*, pages 1065–1185, 2005.

[24] Shapiro Mikhail G, Atanasijevic Tatjana, Faas Henryk, Westmeyer Gil G, and Jasanoff Alan. Dynamic imaging with mri contrast agents: quantitative considerations. *Magnetic resonance imaging*, 24(4):449–462, 2006.

[25] Bowen Chris V, Zhang Xiaowei, Saab George, Gareau Paula J, and Rutt Brian K. Application of the static dephasing regime theory to superparamagnetic iron-oxide loaded cells. *Magnetic resonance in medicine*, 48(1):52–61, 2002.

[26] Gossuin Yves, Roch Alain, Muller Robert N, and Gillis Pierre. An evaluation of the contributions of diffusion and exchange in relaxation enhancement by mri contrast agents. *Journal of Magnetic Resonance*, 158(1):36–42, 2002.

[27] Beckman Coulter, Inc. *PCS Software Help Manual*, 2003.

[28] Hak Sjoerd, Helgesen Emily, Hektoen Helga H, Huuse Else Marie, Jarzyna Peter A, Mulder Willem JM, Haraldseth Olav, and Davies Catharina de Lange. The effect of nanoparticle polyethylene glycol surface density on ligand-directed tumor targeting studied in vivo by dual modality imaging. *Acs Nano*, 6(6):5648–5658, 2012.

[29] Matthew Kramer. R2 statistics for mixed models. In *Proceedings of the Conference on Applied Statistics in Agriculture*, volume 17, pages 148–160, 2005.

[30] De Gennes PG. Polymers at an interface; a simplified view. *Advances in Colloid and Interface Science*, 27(3):189–209, 1987.

[31] Hansen Per Lyngs, Cohen Joel A, Podgornik Rudi, and Parsegian V Adrian. Osmotic properties of poly (ethylene glycols): quantitative features of brush and bulk scaling laws. *Biophysical journal*, 84(1):350–355, 2003.

[32] Chantal Paquet, Hendrick W de Haan, Donald M Leek, Hung-Yu Lin, Bo Xiang, Ganghong Tian, Arnold Kell, and Benoit Simard. Clusters of superparamagnetic iron oxide nanoparticles encapsulated in a hydrogel: a particle architecture generating a synergistic enhancement of the t2 relaxation. *ACS nano*, 5(4):3104–3112, 2011.

[33] Hua Ai, Christopher Flask, Brent Weinberg, X-T Shuai, Marty D Pagel, David Farrell, Jeffrey Duerk, and Jinming Gao. Magnetite-loaded polymeric micelles as ultrasensitive magnetic-resonance probes. *Advanced Materials*, 17(16):1949–1952, 2005.

[34] BA Larsen, MA Haag, NJ Serkova, KR Shroyer, and CR Stoldt. Controlled aggregation of superparamagnetic iron oxide nanoparticles for the development of molecular magnetic resonance imaging probes. *Nanotechnology*, 19(26):265102, 2008.

[35] Sheng Tong, Sijian Hou, Zhilan Zheng, Jun Zhou, and Gang Bao. Coating optimization of superparamagnetic iron oxide nanoparticles for high t2 relaxivity. *Nano letters*, 10(11):4607–4613, 2010.

[36] Alexey Stepanov, Vladimir Burilov, Marina Pinus, Asiya Mustafina, Mark H Rümmeli, Rafael G Mendez, Rustem Amirov, Svetlana Lukashenko, Elena Zvereva, Sergey Katsuba, et al. Water transverse relaxation rates in aqueous dispersions of superparamagnetic iron oxide nanoclusters with diverse hydrophilic coating. *Colloids and Surfaces A: Physicochemical and Engineering Aspects*, 443:450–458, 2014.

[37] Yves Gossuin, Pierre Gillis, Aline Hocq, Quoc L Vuong, and Alain Roch. Magnetic resonance relaxation properties of superparamagnetic particles. *Wiley Interdisciplinary Reviews: Nanomedicine and Nanobiotechnology*, 1(3):299–310, 2009.

[38] Jeff WM Bulte, Josef Vymazal, Rodney A Brooks, Carlo Pierpaoli, and Joseph A Frank. Frequency dependence of mr relaxation times ii. iron oxides. *Journal of Magnetic Resonance Imaging*, 3(4):641–648, 1993.

Appendix

A1: Excel sheet for the mixing ratio

Soybean oil							
P10				Needed from stock:			
				25 mg/ml	100 mg/ml	500 mg/ml	
	Molar ratio	MW	Amount (mg)				
DSPC	0.9	790	3.56	0.142	0.036		ml
Cholesterol	0.33	386	0.64	0.025	0.006		ml
PEG-DSPE	0.1	2806	1.40	0.056	0.014		ml
Soybean oil (mg/umole)	2.4		11.925	0.477	0.119	0.024	ml
				Needed from stock:			
				10 mg/ml	5 mg/ml		
Fe3O4 (mg)			0.417121047	0.017	0.083		
Total amount needed:		5	µmol	lipid			
Calculations							
Fe3O4		volume (m3)					
Nr of FeO-nps/droplet	50	6.54498E-26	m3				
Soybean oil volume/umole lipid		2.61723E-09	m3				
100 nm droplet volume		5.23599E-22	m3				
nr of droplets/umole lipid		4.99854E+12	-				
Nr of FeO-nps/umole lipid		2.49927E+14	-				
volume of FeO-nps/umole lipid		1.63577E-11	m3				
Volume of soybean oil/umole lipid		2.60087E-09	m3				
mg of soybean oil/umole lipid		2.385	mg/umole lipid				
Soybean oil to add		11.925					
FeO-np mass		3.33794E-22	kg				
FeO mass to add/umole lipid		8.34242E-08	kg				
Total FeO mass to add/umole lipid		4.17121E-07					
		0.417121047	mg				

Soybean oil							
P50				Needed from stock:			
				25 mg/ml	100 mg/ml	500 mg/ml	
	Molar ratio	MW	Amount (mg)				
DSPC	0.5	790	1.98	0.079	0.020		ml
Cholesterol	0.33	386	0.64	0.025	0.006		ml
PEG-DSPE	0.5	2806	7.02	0.281	0.070		ml
Soybean oil (mg/umole)	5.3		26.334375	1.053	0.263	0.053	ml
				Needed from stock:			
				10 mg/ml	5 mg/ml		
Fe3O4 (mg)			0.921142312	0.037	0.184		
Total amount needed:		5	µmol	lipid			
Calculations							
Fe3O4		volume (m3)					
Nr of FeO-nps/droplet	50	6.54498E-26	m3				
Soybean oil volume/umole lipid		5.77972E-09	m3				
100 nm droplet volume		5.23599E-22	m3				
nr of droplets/umole lipid		1.10384E+13	-				
Nr of FeO-nps/umole lipid		5.51922E+14	-				
volume of FeO-nps/umole lipid		3.61232E-11	m3				
Volume of soybean oil/umole lipid		5.74359E-09	m3				
mg of soybean oil/umole lipid		5.266875	mg/umole lipid				
Soybean oil to add		26.334375					
FeO-np mass		3.33794E-22	kg				
FeO mass to add/umole lipid		1.84228E-07	kg				
Total FeO mass to add/umole lipid		9.21142E-07					
		0.921142312	mg				

A2: Fit graphs

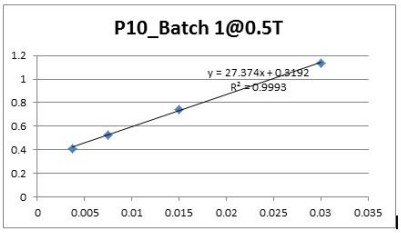
P10_Batch 1@0.5T
y = 27.374x + 0.3192
R² = 0.9993

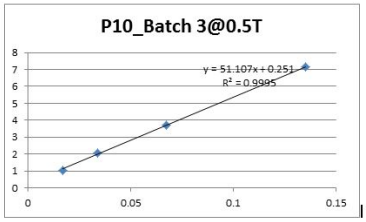
P10_Batch 3@0.5T
y = 51.107x + 0.251
R² = 0.9995

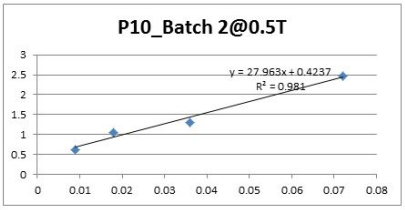
P10_Batch 2@0.5T
y = 27.963x + 0.4237
R² = 0.981

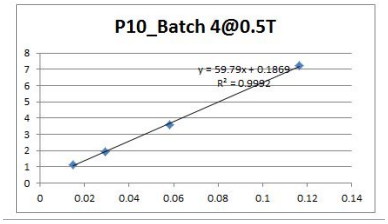
P10_Batch 4@0.5T
y = 59.79x + 0.1869
R² = 0.9982

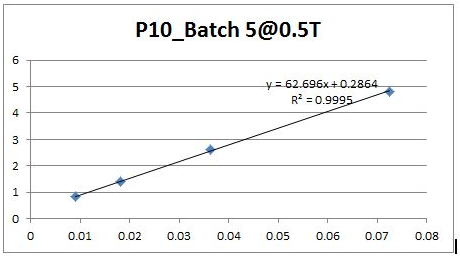
P10_Batch 5@0.5T
y = 62.696x + 0.2864
R² = 0.9995

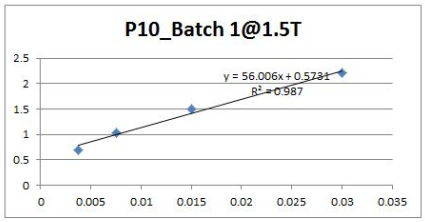
P10_Batch 1@1.5T
y = 56.006x + 0.5731
R² = 0.987

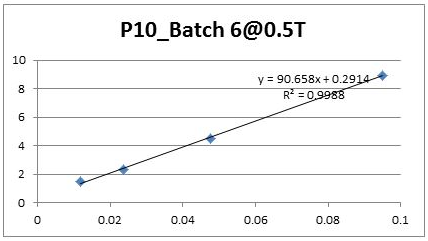
P10_Batch 6@0.5T
y = 90.658x + 0.2914
R² = 0.9988

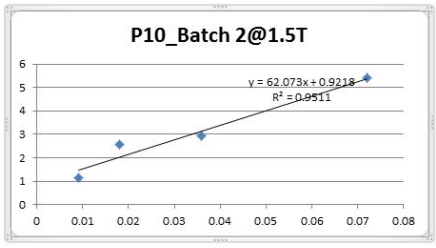
P10_Batch 2@1.5T
y = 62.073x + 0.9218
R² = 0.9511

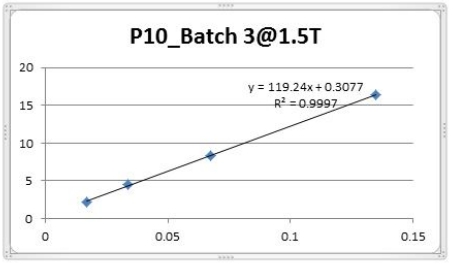
P10_Batch 3@1.5T
y = 119.24x + 0.3077
R² = 0.9997
20
15
10
5
0
0
0.05
0.1
0.15

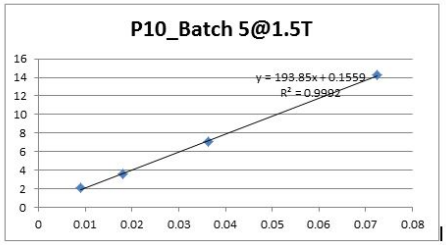
P10_Batch 5@1.5T
y = 193.85x + 0.1559
R² = 0.9992
16
14
12
10
8
6
4
2
0
0
0.01
0.02
0.03
0.04
0.05
0.06
0.07
0.08

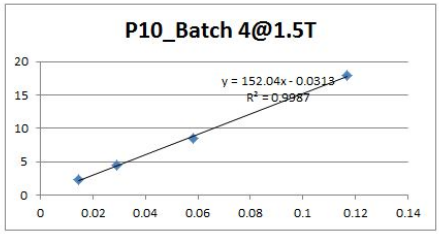
P10_Batch 4@1.5T
y = 152.04x - 0.0313
R² = 0.9987
20
15
10
5
0
0
0.02
0.04
0.06
0.08
0.1
0.12
0.14

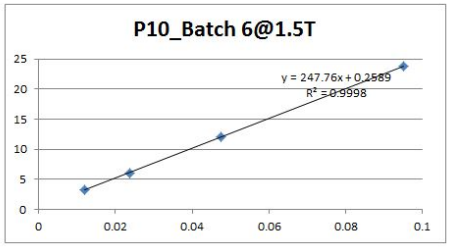
P10_Batch 6@1.5T
y = 247.76x + 0.2589
R² = 0.9998
25
20
15
10
5
0
0
0.02
0.04
0.06
0.08
0.1

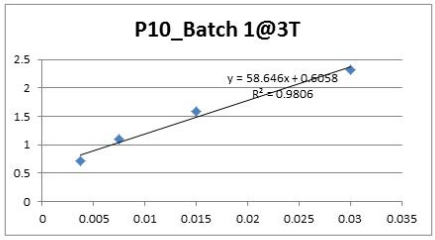
P10_Batch 1@3T
y = 58.646x + 0.6058
R² = 0.9806
2.5
2
1.5
1
0.5
0
0
0.005
0.01
0.015
0.02
0.025
0.03
0.035

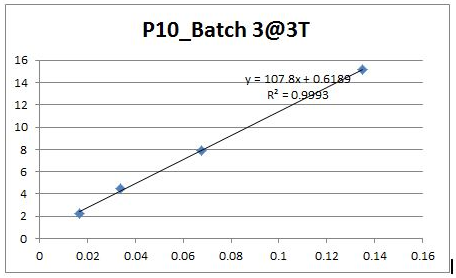
P10_Batch 3@3T
y = 107.8x + 0.6189
R² = 0.9993
16
14
12
10
8
6
4
2
0
0
0.02
0.04
0.06
0.08
0.1
0.12
0.14
0.16

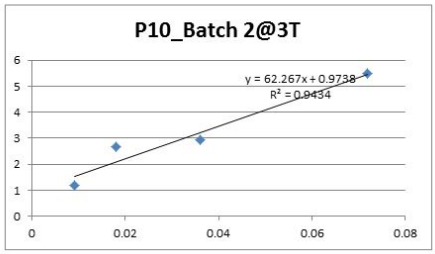
P10_Batch 2@3T
y = 62.267x + 0.9738
R² = 0.9434
6
5
4
3
2
1
0
0
0.02
0.04
0.06
0.08

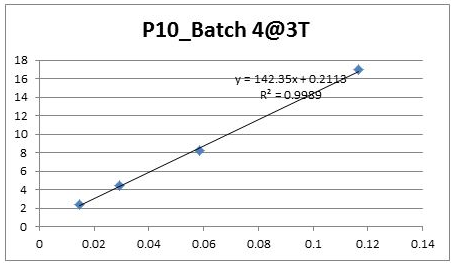
P10_Batch 4@3T
y = 142.35x + 0.2113
R² = 0.9989
18
16
14
12
10
8
6
4
2
0
0
0.02
0.04
0.06
0.08
0.1
0.12
0.14

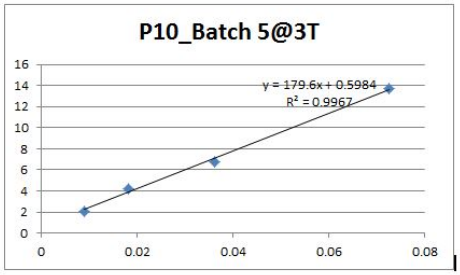
P10_Batch 5@3T
y = 179.6x + 0.5984
R² = 0.9967

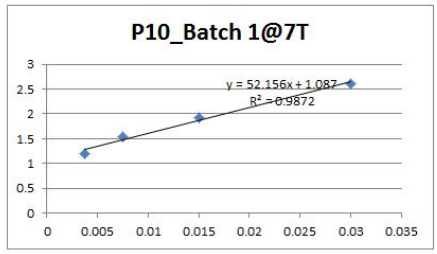
P10_Batch 1@7T
y = 52.156x + 1.087
R² = 0.9872

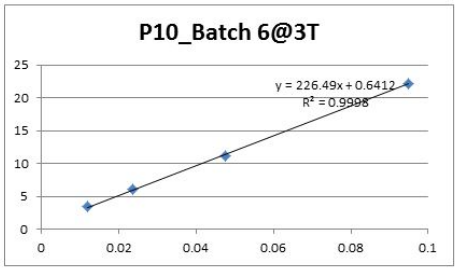
P10_Batch 6@3T
y = 226.49x + 0.6412
R² = 0.9998

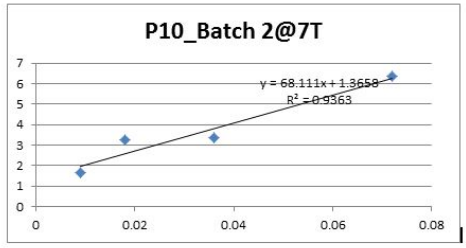
P10_Batch 2@7T
y = 68.111x + 1.3658
R² = 0.9363

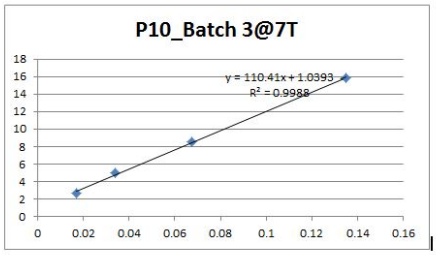
P10_Batch 3@7T
y = 110.41x + 1.0393
R² = 0.9988

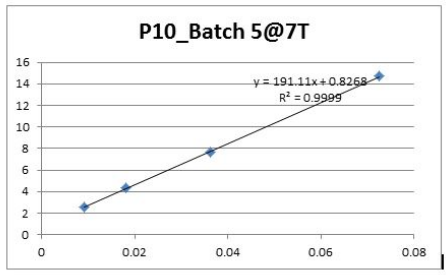
P10_Batch 5@7T
y = 191.11x + 0.8268
R² = 0.9999

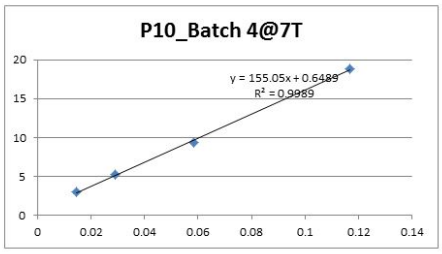
P10_Batch 4@7T
y = 155.05x + 0.6489
R² = 0.9989

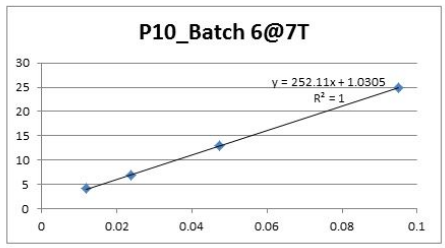
P10_Batch 6@7T
y = 252.11x + 1.0305
R² = 1

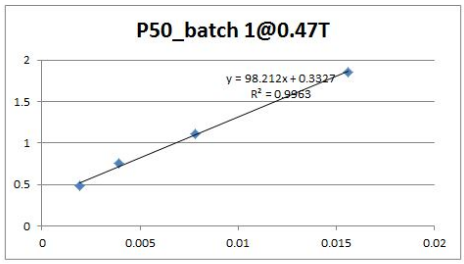
P50_batch 1@0.47T
y = 98.212x + 0.3327
R² = 0.9963

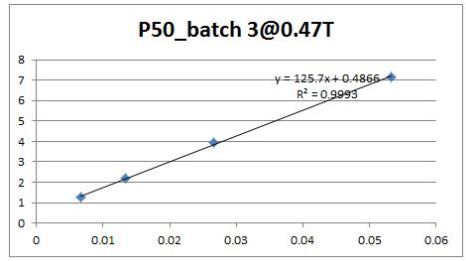
P50_batch 3@0.47T
y = 125.7x + 0.4866
R² = 0.9993

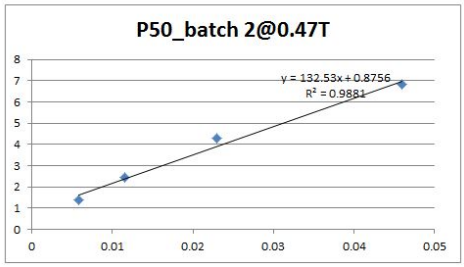
P50_batch 2@0.47T
y = 132.53x + 0.8756
R² = 0.9881

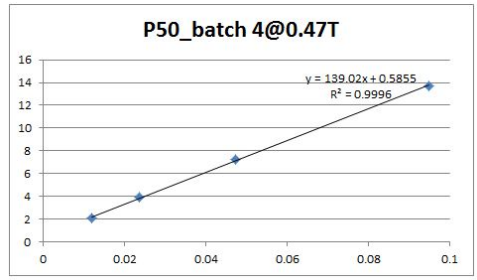
P50_batch 4@0.47T
y = 139.02x + 0.5855
R² = 0.9996

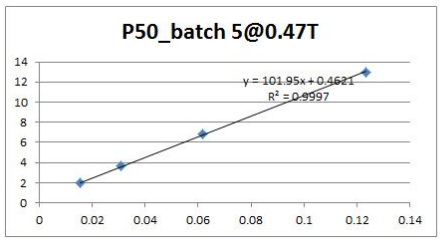
P50_batch 5@0.47T
y = 101.95x + 0.4621
R² = 0.9997

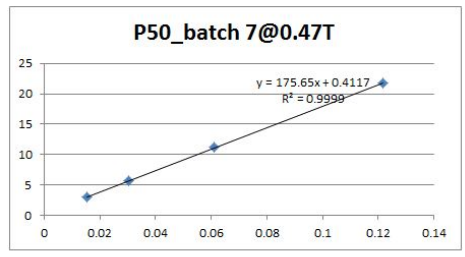
P50_batch 7@0.47T
y = 175.65x + 0.4117
R² = 0.9999

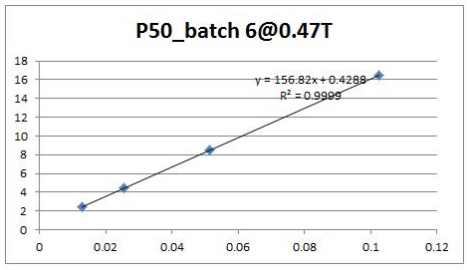
P50_batch 6@0.47T
y = 156.82x + 0.4288
R² = 0.9989

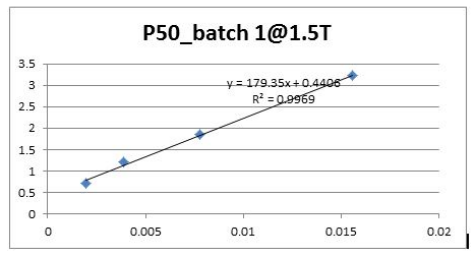
P50_batch 1@1.5T
y = 179.35x + 0.4406
R² = 0.9969

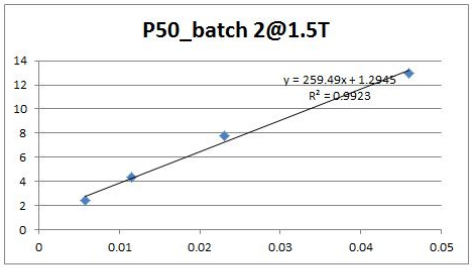
P50_batch 2@1.5T
y = 259.49x + 1.2945
R² = 0.9923

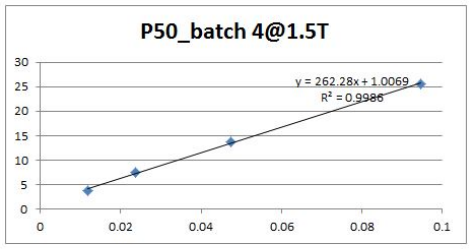
P50_batch 4@1.5T
y = 262.28x + 1.0069
R² = 0.9986

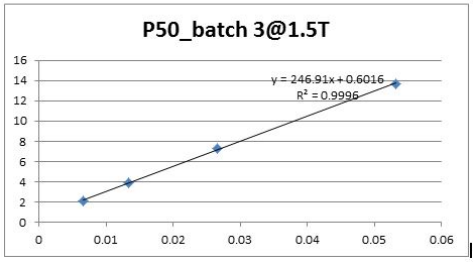
P50_batch 3@1.5T
y = 246.91x + 0.6016
R² = 0.9996

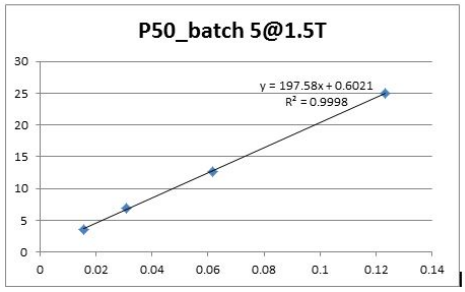
P50_batch 5@1.5T
y = 197.58x + 0.6021
R² = 0.9998

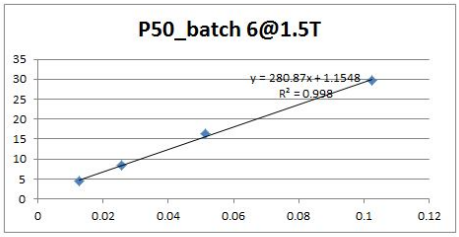
P50_batch 6@1.5T
y = 280.87x + 1.1548
R² = 0.998

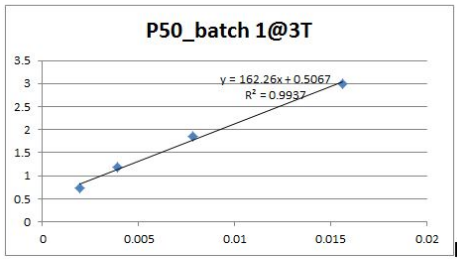
P50_batch 1@3T
y = 162.26x + 0.5067
R² = 0.9937

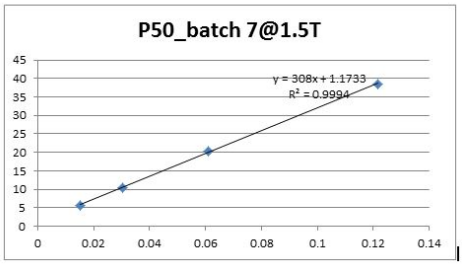
P50_batch 7@1.5T
y = 308x + 1.1733
R² = 0.9994

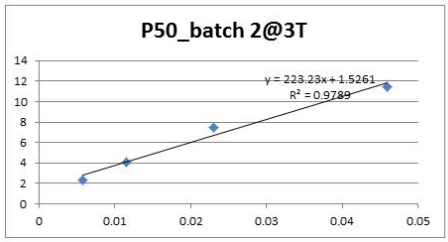
P50_batch 2@3T
y = 223.23x + 1.5261
R² = 0.9789

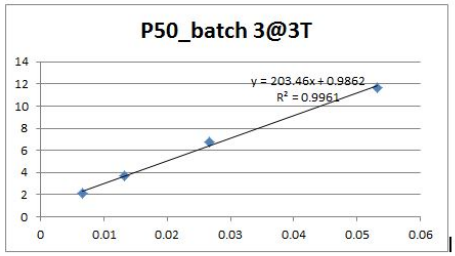
P50_batch 3@3T
y = 203.46x + 0.9862
R² = 0.9961

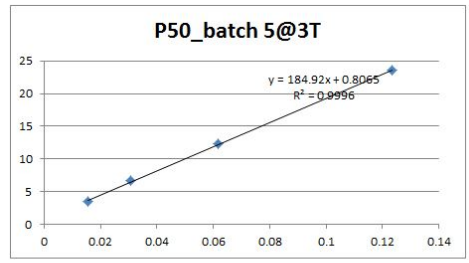
P50_batch 5@3T
y = 184.92x + 0.8065
R² = 0.9996

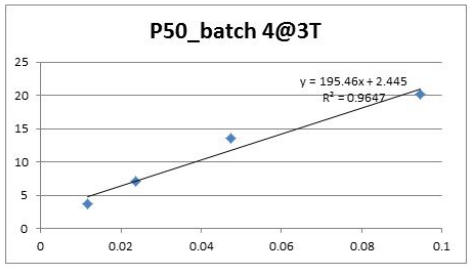
P50_batch 4@3T
y = 195.46x + 2.445
R² = 0.9647

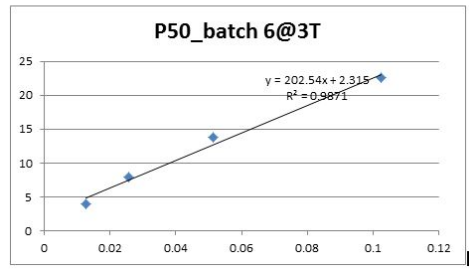
P50_batch 6@3T
y = 202.54x + 2.315
R² = 0.9871

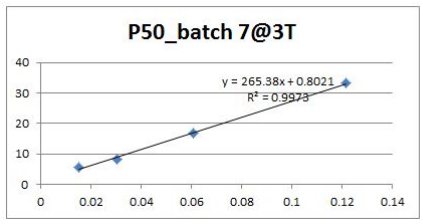
P50_batch 7@3T
y = 265.38x + 0.8021
R² = 0.9973

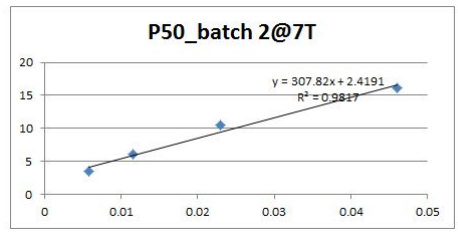
P50_batch 2@7T
y = 307.82x + 2.4191
R² = 0.9817

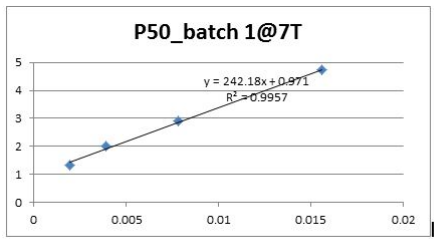
P50_batch 1@7T
y = 242.18x + 0.971
R² = 0.9957

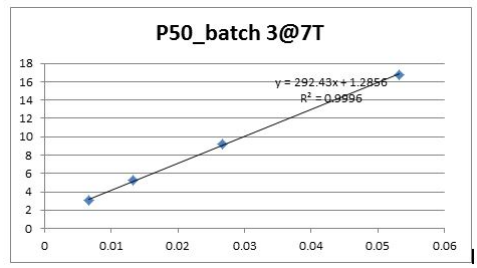
P50_batch 3@7T
y = 292.43x + 1.2856
R² = 0.9996

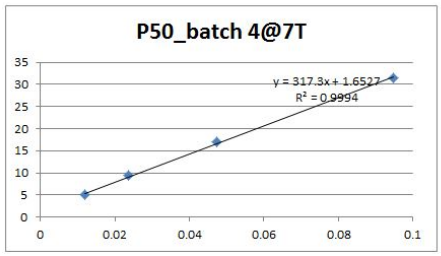
P50_batch 4@7T
y = 317.3x + 1.6527
R² = 0.9994
35
30
25
20
15
10
5
0
0
0.02
0.04
0.06
0.08
0.1

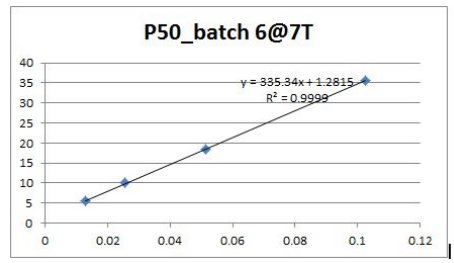
P50_batch 6@7T
y = 335.34x + 1.2815
R² = 0.9998
40
35
30
25
20
15
10
5
0
0
0.02
0.04
0.06
0.08
0.1
0.12

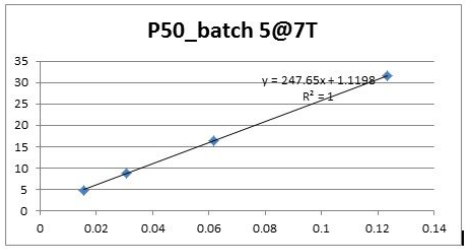
P50_batch 5@7T
y = 247.65x + 1.1198
R² = 1
35
30
25
20
15
10
5
0
0
0.02
0.04
0.06
0.08
0.1
0.12
0.14

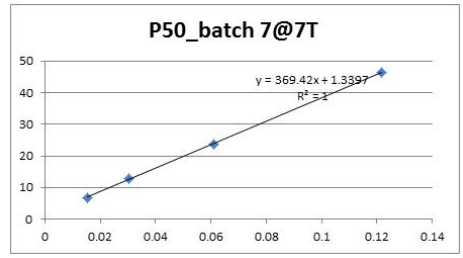
P50_batch 7@7T
y = 369.42x + 1.3397
R² = 1
50
40
30
20
10
0
0
0.02
0.04
0.06
0.08
0.1
0.12
0.14

A3: Matlab code for model fitting

```
%function r2_comparison
% First need to establish experimental data:
% For each measured r2 we need to know:
%
% L,r,f,D,Beq,n,R

clear
close all

%% First compare vuong to our implementation:
% Fe volume fraction:
r = 2.5e-9;
f = 3.14e-6;
D = 3e-9;
Beq = 0.16;
%R2_vuong = Relaxationrate_R2_outersphere(r,f,D,Beq)
%r2_vuong = 4.74*R2_vuong


VolIONC = 4.*pi.*r.^3./3;
m  =  4.33e-21 ./ VolIONC; % mol/m^3 = mM
r2_palgo = relaxivity_r2_outersphere(r,D,Beq,m)

% IONC magnetic moment:
mu = 1.36e-20; %Am^2 From manufacturer
vacuumPerm = 4*pi*1e-7; % H/m
Beq = (mu.*vacuumPerm)./(4.*pi.*r.^3) %From equation 2 from Vuong, and magnetic moment of the IONC
r2_IONC_max = relaxivity_r2_outersphere(r,D,Beq,m)
```

```

%% Model calculations for our experimental system:

% Data sorting:
% 1:6 p10,batch 1 0.47 T
% 7:12 p10,batch 2 1.5 T
% 13:18 p10,batch 3 0.47 T
% 19:24 p10,batch 4 0.47 T
% 25:31 p50,batch 1 0.47 T
% 32:38 p50,batch 2 1.5 T
% 39:45 p50,batch 3 3 T
% 46:52 p50,batch 4 7 T

% IONC magnetic moment:
mu = 1.36e-20; %Am^2
vacuumPerm = 4*pi*1e-7; % H/m

% Experimental temperatures (K):
Ta = 313; % (40oc at 0.47T (minispec))
Tb = 294; % ( room temperature (21oc) at 1.5T scanner)
Tc = 294; % ( room temperature (21oc) at 3T scanner)
Td = 294; % ( room temperature (21oc) at 7T scanner)

% Langevin factors:
La = Langevin(mu,0.47,Ta); % 0.47 T
Lb = Langevin(mu,1.5,Tb); % 1.5 T
Lc = Langevin(mu,3,Tc);   % 3 T
Ld = Langevin(mu,7,Td);   % 7 T
L =  [La.*ones(1,6) Lb.*ones(1,6) Lc.*ones(1,6) Ld.*ones(1,6) La.*ones(1,7) Lb.*ones(1,7) Lc.*ones(1,7) Ld.*ones(1,7)];
```

```
61
62      % IONC radius:
63 -    r = 2.5e-9.*ones(1,52);
64
65      % Water diffusion constants:
66 -    D = [3e-9.*ones(1,6) 2.3e-9.*ones(1,6)  2.3e-9.*ones(1,6) 2.3e-9.*ones(1,6) 3e-9.*ones(1,7) 2.3e-9.*ones(1,7) 2.3e-9.*ones(1,7) 2.3e-9.*ones(1,7)];
67
68
69      % IONC equatorial field:
70 -    Beq = (mu.*vacuumPerm)./(4.*pi.*r.^3); %From equation 2 from Vuong, and magnetic moment of the IONC
71
72      % Mol Fe per unit volume of IONC crystals:
73 -    VolIONC = 4.*pi.*r.^3./3;
74 -    m  =  4.33e-21 ./ VolIONC; % mol/m^3 = mM
75
76      % Number of IONC per NE droplet:
77 -    n  = [0.916 1.99 4.84 10.3 22 20.1 ...
78            0.916 1.99 4.84 10.3 22 20.1 ...
79            0.916 1.99 4.84 10.3 22 20.1 ...
80            0.916 1.99 4.84 10.3 22 20.1 ...
81            0.25 1.1 1.85 6.46 9.87 19.75 41.3 ...
82            0.25 1.1 1.85 6.46 9.87 19.75 41.3 ...
83            0.25 1.1 1.85 6.46 9.87 19.75 41.3 ...
84            0.25 1.1 1.85 6.46 9.87 19.75 41.3 ];
```

```
85      % NE droplet radius(m):
86 -    R  = 0.5e-9 .*[103 105 109.5 109 108 95.5 ...
87                     103 105 109.5 109 108 95.5 ...
88                     103 105 109.5 109 108 95.5 ...
89                     103 105 109.5 109 108 95.5 ...
90                     97 105 98 107 97 106 108 ...
91                     97 105 98 107 97 106 108 ...
92                     97 105 98 107 97 106 108 ...
93                     97 105 98 107 97 106 108 ] - 3.77e-9;
94
95      % Measured relaxivities (units of mM^-1s^-1)
96 -    r2exp = [27 28 51 60 63 90 ...
97             56 62 119 152 194 248 ...
98             59 62 108 142 179 226 ...
99             52 68 110 155 191 252 ...
100            98 132 126 139 102 157 175 ...
101            179 259 247 262 197 281 308 ...
102            162 223 203 195 185 202 265 ...
103            242 308 292 317 248 335 369 ];
104
```

```
106 -   load dlsmeas
107
108 -   NErdelta = 1e-9;
109 -   NEr = [1e-9:NErdelta:200e-9]';
110 -   for k = 1:numel(NEr)
111 -       for s = 1:52
112 -           if s <=6
113 -               NErprob(k,s) = interp1(dlsp10r,dlsp10pdf(:,s),NEr(k),'linear');
114 -           elseif s<=12
115 -               NErprob(k,s) = interp1(dlsp10r,dlsp10pdf(:,s-6),NEr(k),'linear');
116 -           elseif s<=18
117 -               NErprob(k,s) = interp1(dlsp10r,dlsp10pdf(:,s-12),NEr(k),'linear');
118 -           elseif s<=24
119 -               NErprob(k,s) = interp1(dlsp10r,dlsp10pdf(:,s-18),NEr(k),'linear');
120 -           elseif s<=31
121 -               NErprob(k,s) = interp1(dlsp50r,dlsp50pdf(:,s-24),NEr(k),'linear');
122 -           elseif s<=38
123 -               NErprob(k,s) = interp1(dlsp50r,dlsp50pdf(:,s-31),NEr(k),'linear');
124 -           elseif s<=45
125 -               NErprob(k,s) = interp1(dlsp50r,dlsp50pdf(:,s-38),NEr(k),'linear');
126 -           else
127 -               NErprob(k,s) = interp1(dlsp50r,dlsp50pdf(:,s-45),NEr(k),'linear');
128 -           end
129 -       end
130 -   end
131 -   NErprob(find(isnan(NErprob))) = 0;
132 -   for k = 1:52
133 -       NErprob(:,k) = NErprob(:,k)./trapz(NEr,NErprob(:,k) );
134 -   end
```

```
136
137     % Calculate theoretical relaxivities for four different outer sphere
138     % models:
139
140     %% First without polydispersity:
141 -   for k = 1:numel(L)
142         % Uniform distribution of IONC:
143 -       r2_iso(k) = relaxivity_r2_outersphere(r(k),D(k),L(k)*Beq(k),m(k));
144 -       r2star_iso(k) = relaxivity_r2star_static(L(k)*Beq(k),m(k));
145
146         % Dense cluster of n IONC:
147 -       Reff_dense(k) = r(k) .* ((4.24.*n(k)./pi).^(1/3));
148 -       meff_dense(k) = m(k) * pi/4.24;
149 -       Beqeff_dense(k) =  Beq(k) * pi/4.24;
150 -       r2_dense(k) = relaxivity_r2_outersphere(Reff_dense(k),D(k),L(k)*Beqeff_dense(k),meff_dense(k));
151 -       r2star_dense(k) = relaxivity_r2star_static(L(k)*Beqeff_dense(k),meff_dense(k));
152
153         % Uniform distribution inside NE droplet:
154 -       Reff_ne(k) = R(k);
155 -       Volratio(k) = n(k) * r(k)^3 / Reff_ne(k)^3;
156 -       meff_ne(k) = m(k)  * Volratio(k);
157 -       Beqeff_ne(k) = Beq(k) * Volratio(k);
158 -       r2_ne(k) = relaxivity_r2_outersphere(Reff_ne(k),D(k),L(k)*Beqeff_ne(k),meff_ne(k));
159 -       r2star_ne(k) = relaxivity_r2star_static(L(k)*Beqeff_ne(k),meff_ne(k));
160
161 -   end
```

```
    % Then with polydispersity

for k = 1:numel(L)
    for q = 1:numel(NEr)
        neff_poly(k,q) = n(k) * (NEr(q)/R(k))^3;
        % Dense cluster of n IONC:
        Reff_dense_poly(k,q) = r(k) .* ((4.24.*neff_poly(k,q)./pi).^(1/3));
        r2_dense_poly(k,q) = relaxivity_r2_outersphere(Reff_dense_poly(k,q),D(k),L(k)*Beqeff_dense(k),meff_dense(k));

        % Uniform distribution inside NE droplet:
        Reff_ne_poly(k,q) = NEr(q);
        Volratio_poly(k,q) = neff_poly(k,q) * r(k)^3 / Reff_ne_poly(k,q)^3;
        meff_ne_poly(k,q) = m(k)  * Volratio_poly(k,q);
        Beqeff_ne_poly(k,q) = Beq(k) * Volratio_poly(k,q);
        r2_ne_poly(k,q) = relaxivity_r2_outersphere(Reff_ne_poly(k,q),D(k),L(k)*Beqeff_ne_poly(k,q),meff_ne_poly(k,q));
        r2star_ne_poly(k,q) = relaxivity_r2star_static(L(k)*Beqeff_ne_poly(k,q),meff_ne_poly(k,q));
    end
    r2_dense_poly_eff(k) = trapz(NEr,r2_dense_poly(k,:).*NErprob(:,k)');
    r2_ne_poly_eff(k) = trapz(NEr,r2_ne_poly(k,:).*NErprob(:,k)');
    r2star_ne_poly_eff(k) = trapz(NEr,r2star_ne_poly(k,:).*NErprob(:,k)');

end
```

```
%% Some plotting of the results:

a = 1:6;
b = 7:12;
c = 13:18;
d = 19:24;
e = 25:31;
f = 32:38;
g = 39:45;
h = 46:52;
textfont = 12;
textweight = 'b';


subplot(2,2,1)
loglog(n(a),r2exp(a),'+', n(a),r2_iso(a),n(a),r2_dense(a), n(a),r2_dense_poly_eff(a),n(a),r2_ne(a), n(a), r2_ne_poly_eff(a), n(a), r2star_iso(a),'Linewidth',
%xlim([0.5,100]), ylim([1,1000])
xlabel('(a)','Fontsize',textfont,'FontWeight',textweight)
ylabel('Relaxivity r2 [mM-1 s-1]','Fontsize',textfont,'FontWeight',textweight)
%title('p10 at 0.47 T','Fontsize',textfont,'FontWeight',textweight)
legend('Exp','Isotropic','DA','DA with poly','LA','LA with poly.','Static','Fontsize',textfont,'FontWeight',textweight)
set(gca,'FontSize',textfont)
```

```
subplot(2,2,3)%, loglog(n(b),r2exp(b),'+', n(b),r2_iso(b), n(b),r2_dense(b),n(b),r2_ne(b), n(b), r2star_iso(b), 'Linewidth', 1.5)
loglog(n(b),r2exp(b),'+', n(b),r2_iso(b), n(b),r2_dense(b), n(b),r2_dense_poly_eff(b),n(b),r2_ne(b), n(b), r2_ne_poly_eff(b), n(b), r2star_iso(b),'Linewidth'
%xlim([0.5,100]), ylim([1,1000])
xlabel('(c)            Number of IONC per nanoemulsion droplet','Fontsize',textfont,'FontWeight',textweight)
%ylabel('Relaxivity r2 [mM-1 s-1]','Fontsize',textfont,'FontWeight',textweight)
%title('p10 at 1.5 T','Fontsize',textfont,'FontWeight',textweight)

subplot(2,2,2)%, loglog(n(c),r2exp(c),'+', n(c),r2_iso(c), n(c),r2_dense(c),n(c),r2_ne(c), n(c), r2star_iso(c), 'Linewidth',1.5)
loglog(n(c),r2exp(c),'+', n(c),r2_iso(c),n(c),r2_dense(c), n(c),r2_dense_poly_eff(c),n(c),r2_ne(c), n(c), r2_ne_poly_eff(c), n(c), r2star_iso(c),'Linewidth',
%xlim([0.5,100]), ylim([1,1000])
xlabel('(b)','Fontsize',textfont,'FontWeight',textweight)
%ylabel('Relaxivity r2 [mM-1 s-1]','Fontsize',textfont,'FontWeight',textweight)
%title('p10 at 3 T','Fontsize',textfont,'FontWeight',textweight)

subplot(2,2,4)%, loglog(n(d),r2exp(d),'+', n(d),r2_iso(d), n(d),r2_dense(d),n(d),r2_ne(d), n(d), r2star_iso(d), 'Linewidth',1.5)
loglog(n(d),r2exp(d),'+', n(d),r2_iso(d),n(d),r2_dense(d), n(d),r2_dense_poly_eff(d),n(d),r2_ne(d), n(d), r2_ne_poly_eff(d), n(d), r2star_iso(d),'Linewidth',
%xlim([0.5,100]), ylim([1,1000])
xlabel('(d)','Fontsize',textfont,'FontWeight',textweight)
%ylabel('Relaxivity r2 [mM-1 s-1]','Fontsize',textfont,'FontWeight',textweight)
%title('p10 at 7 T','Fontsize',textfont,'FontWeight',textweight)
subplot(2,2,1)
loglog(n(a),r2exp(a),'+', n(a),r2_iso(a),n(a),r2_dense(a), n(a),r2_ne(a), n(a), r2star_iso(a),'Linewidth', 1.5)
%xlim([0.5,100]), ylim([1,1000])
xlabel('(a) Number of IONC per nanoemulsion droplet')
ylabel('Relaxivity r2 [mM-1 s-1]')
title('p10 at 0.47 T')
legend('Exp','Isotropic','DA','LA','Static')
set(gca,'FontSize',textfont)
```

```
subplot(2,2,3)%, loglog(n(b),r2exp(b),'+', n(b),r2_iso(b), n(b),r2_dense(b),n(b),r2_ne(b), n(b), r2star_iso(b), 'Linewidth', 1.5)
loglog(n(b),r2exp(b),'+', n(b),r2_iso(b), n(b),r2_dense(b),n(b),r2_ne(b), n(b), r2star_iso(b),'Linewidth', 1.5)
%xlim([0.5,100]), ylim([1,1000])
xlabel('(c) Number of IONC per nanoemulsion droplet')
ylabel('Relaxivity r2 [mM-1 s-1]')
title('p10 at 1.5 T')

subplot(2,2,2)%, loglog(n(c),r2exp(c),'+', n(c),r2_iso(c), n(c),r2_dense(c),n(c),r2_ne(c), n(c), r2star_iso(c), 'Linewidth',1.5)
loglog(n(c),r2exp(c),'+', n(c),r2_iso(c),n(c),r2_dense(c), n(c),r2_ne(c), n(c), r2star_iso(c),'Linewidth', 1.5)
%xlim([0.5,100]), ylim([1,1000])
xlabel('(b) Number of IONC per nanoemulsion droplet')
ylabel('Relaxivity r2 [mM-1 s-1]')
title('p10 at 3 T')

subplot(2,2,4)%, loglog(n(d),r2exp(d),'+', n(d),r2_iso(d), n(d),r2_dense(d),n(d),r2_ne(d), n(d), r2star_iso(d), 'Linewidth',1.5)
loglog(n(d),r2exp(d),'+', n(d),r2_iso(d),n(d),r2_dense(d), n(d),r2_ne(d), n(d), r2star_iso(d),'Linewidth', 1.5)
%xlim([0.5,100]), ylim([1,1000])
xlabel('(d) Number of IONC per nanoemulsion droplet')
ylabel('Relaxivity r2 [mM-1 s-1]')
title('p10 at 7 T')
subplot(2,2,1)
loglog(n(a),r2exp(a),'+', n(a),r2_iso(a), n(a),r2_dense_poly_eff(a), n(a), r2_ne_poly_eff(a), n(a), r2star_iso(a),'Linewidth', 1.5)
%xlim([0.5,100]), ylim([1,1000])
xlabel('(a) Number of IONC per nanoemulsion droplet')
ylabel('Relaxivity r2 [mM-1 s-1]')
title('p10 at 0.47 T')
legend('Exp','Isotropic','DA with polydisp','LA with polydisp.','Static')
set(gca,'FontSize',textfont)
```

```
subplot(2,2,3)%, loglog(n(b),r2exp(b),'+', n(b),r2_iso(b), n(b),r2_dense(b),n(b),r2_ne(b), n(b), r2star_iso(b), 'Linewidth', 1.5)
loglog(n(b),r2exp(b),'+', n(b),r2_iso(b), n(b),r2_dense_poly_eff(b), n(b), r2_ne_poly_eff(b), n(b), r2star_iso(b),'Linewidth', 1.5)
%xlim([0.5,100]), ylim([1,1000])
xlabel('(c) Number of IONC per nanoemulsion droplet')
ylabel('Relaxivity r2 [mM-1 s-1]')
title('p10 at 1.5 T')

subplot(2,2,2)%, loglog(n(c),r2exp(c),'+', n(c),r2_iso(c), n(c),r2_dense(c),n(c),r2_ne(c), n(c), r2star_iso(c), 'Linewidth',1.5)
loglog(n(c),r2exp(c),'+', n(c),r2_iso(c), n(c),r2_dense_poly_eff(c), n(c), r2_ne_poly_eff(c), n(c), r2star_iso(c),'Linewidth', 1.5)
%xlim([0.5,100]), ylim([1,1000])
xlabel('(b) Number of IONC per nanoemulsion droplet')
ylabel('Relaxivity r2 [mM-1 s-1]')
title('p10 at 3 T')

subplot(2,2,4)%, loglog(n(d),r2exp(d),'+', n(d),r2_iso(d), n(d),r2_dense(d),n(d),r2_ne(d), n(d), r2star_iso(d), 'Linewidth',1.5)
loglog(n(d),r2exp(d),'+', n(d),r2_iso(d), n(d),r2_dense_poly_eff(d), n(d), r2_ne_poly_eff(d), n(d), r2star_iso(d),'Linewidth', 1.5)
%xlim([0.5,100]), ylim([1,1000])
xlabel('(d) Number of IONC per nanoemulsion droplet')
ylabel('Relaxivity r2 [mM-1 s-1]')
title('p10 at 7 T')
subplot(2,2,1)
loglog(n(e),r2exp(e),'+', n(e),r2_iso(e),n(e),r2_dense(e), n(e),r2_dense_poly_eff(e), n(e),r2_ne(e),n(e),r2_ne_poly_eff(e), n(e), r2star_iso(e),'Linewidth', 
xlabel('(a)','Fontsize',textfont,'FontWeight',textweight)
ylabel('Relaxivity r2 [mM-1 s-1]','Fontsize',textfont,'FontWeight',textweight)
%title('p10 at 0.47 T','Fontsize',textfont,'FontWeight',textweight)
legend('Exp','Isotropic','DA','DA with poly','LA','LA with poly.','Static','Fontsize',textfont,'FontWeight',textweight)
set(gca,'FontSize',textfont)
```

```
subplot(2,2,3)
loglog(n(f),r2exp(f),'+', n(f),r2_iso(f),n(f),r2_dense(f), n(f),r2_dense_poly_eff(f), n(f),r2_ne(f),n(f),r2_ne_poly_eff(f), n(f), r2star_iso(f),'Linewidth', 
xlabel('(c)         Number of IONC per nanoemulsion droplet','Fontsize',textfont,'FontWeight',textweight)
%ylabel('Relaxivity r2 [mM-1 s-1]','Fontsize',textfont,'FontWeight',textweight)
%title('p10 at 1.5 T','Fontsize',textfont,'FontWeight',textweight)
subplot(2,2,2)
loglog(n(g),r2exp(g),'+', n(g),r2_iso(g),n(g),r2_dense(g), n(g),r2_dense_poly_eff(g), n(g),r2_ne(g),n(g),r2_ne_poly_eff(g), n(g), r2star_iso(g),'Linewidth', 
xlabel('(b)','Fontsize',textfont,'FontWeight',textweight)
%ylabel('Relaxivity r2 [mM-1 s-1]','Fontsize',textfont,'FontWeight',textweight)
%title('p10 at 3 T','Fontsize',textfont,'FontWeight',textweight)
subplot(2,2,4)
loglog(n(h),r2exp(h),'+', n(h),r2_iso(h),n(h),r2_dense(h), n(h),r2_dense_poly_eff(h), n(h),r2_ne(h),n(h),r2_ne_poly_eff(h), n(h), r2star_iso(h),'Linewidth', 
xlabel('(d)','Fontsize',textfont,'FontWeight',textweight)
%ylabel('Relaxivity r2 [mM-1 s-1]','Fontsize',textfont,'FontWeight',textweight)
%title('p10 at 7 T','Fontsize',textfont,'FontWeight',textweight)
subplot(2,2,1)
loglog(n(e),r2exp(e),'+', n(e),r2_iso(e),n(e),r2_dense(e), n(e),r2_ne(e), n(e), r2star_iso(e),'Linewidth', 1.5)
xlabel('(a) Number of IONC per nanoemulsion droplet')
ylabel('Relaxivity r2 [mM-1 s-1]')
title('p50 at 0.47 T')
legend('Exp','Isotropic','DA','LA','Static')
set(gca,'FontSize',textfont)
subplot(2,2,3)
loglog(n(f),r2exp(f),'+', n(f),r2_iso(f),n(f),r2_dense(f), n(f),r2_ne(f), n(f), r2star_iso(f),'Linewidth', 1.5)
xlabel('(c) Number of IONC per nanoemulsion droplet')
ylabel('Relaxivity r2 [mM-1 s-1]')
title('p50 at 1.5 T')
subplot(2,2,2)
```

```
 subplot(2,2,2)
 loglog(n(g),r2exp(g),'+', n(g),r2_iso(g),n(g),r2_dense(g), n(g),r2_ne(g), n(g), r2star_iso(g),'Linewidth', 1.5)
 xlabel('(b) Number of IONC per nanoemulsion droplet')
 ylabel('Relaxivity r2 [mM-1 s-1]')
 title('p50 at 3 T')
 subplot(2,2,4)
 loglog(n(h),r2exp(h),'+', n(h),r2_iso(h),n(h),r2_dense(h), n(h),r2_ne(h), n(h), r2star_iso(h),'Linewidth', 1.5)
 xlabel('(d) Number of IONC per nanoemulsion droplet')
 ylabel('Relaxivity r2 [mM-1 s-1]')
 title('p50 at 7 T')
 subplot(2,2,1)
 loglog(n(e),r2exp(e),'+', n(e),r2_iso(e), n(e),r2_dense_poly_eff(e), n(e),r2_ne_poly_eff(e), n(e), r2star_iso(e),'Linewidth', 1.5)
 xlabel('(a) Number of IONC per nanoemulsion droplet')
 ylabel('Relaxivity r2 [mM-1 s-1]')
 title('p50 at 0.47 T')
 legend('Exp','Isotropic','DA with polydisp','LA with polydisp.','Static')
 set(gca,'FontSize',textfont)
 subplot(2,2,3)
 loglog(n(f),r2exp(f),'+', n(f),r2_iso(f), n(f),r2_dense_poly_eff(f), n(f),r2_ne_poly_eff(f), n(f), r2star_iso(f),'Linewidth', 1.5)
 xlabel('(c) Number of IONC per nanoemulsion droplet')
 ylabel('Relaxivity r2 [mM-1 s-1]')
 title('p50 at 1.5 T')
 subplot(2,2,2)
 loglog(n(g),r2exp(g),'+', n(g),r2_iso(g), n(g),r2_dense_poly_eff(g), n(g),r2_ne_poly_eff(g), n(g), r2star_iso(g),'Linewidth', 1.5)
 xlabel('(b) Number of IONC per nanoemulsion droplet')
 ylabel('Relaxivity r2 [mM-1 s-1]')
 title('p50 at 3 T')
```

```
 subplot(2,2,4)
 loglog(n(h),r2exp(h),'+', n(h),r2_iso(h), n(h),r2_dense_poly_eff(h), n(h),r2_ne_poly_eff(h), n(h), r2star_iso(h),'Linewidth', 1.5)
 xlabel('(d) Number of IONC per nanoemulsion droplet')
 ylabel('Relaxivity r2 [mM-1 s-1]')
 title('p50 at 7 T')
 return
 figure
  loglog(n(a),r2exp(a),'+', n(a),r2_ne_poly_eff(a),'k+', n(a),r2_ne(a),'Linewidth', 1.5)
 figure
  loglog(n(b),r2exp(b),'+', n(b),r2_ne_poly_eff(b), n(b),r2_ne(b),'Linewidth', 1.5)
 figure
  loglog(n(c),r2exp(c),'+', n(c),r2_ne_poly_eff(c), n(c),r2_ne(c),'Linewidth', 1.5)
  figure
  loglog(n(d),r2exp(d),'+', n(d),r2_ne_poly_eff(d), n(d),r2_ne(d),'Linewidth', 1.5)

  figure
  loglog(n(a),r2exp(a),'+', n(a),r2_dense_poly_eff(a), n(a),r2_dense(a),'Linewidth', 1.5)
 figure
  loglog(n(b),r2exp(b),'+', n(b),r2_dense_poly_eff(b), n(b),r2_dense(b),'Linewidth', 1.5)
 figure
  loglog(n(c),r2exp(c),'+', n(c),r2_dense_poly_eff(c), n(c),r2_dense(c),'Linewidth', 1.5)
  figure
  loglog(n(d),r2exp(d),'+', n(d),r2_dense_poly_eff(d), n(d),r2_dense(d),'Linewidth', 1.5)
  figure
  loglog(n(e),r2exp(a),'+', n(e),r2_ne_poly_eff(e),'k+', n(e),r2_ne(e),'Linewidth', 1.5)
 figure
  loglog(n(f),r2exp(f),'+', n(f),r2_ne_poly_eff(f), n(f),r2_ne(f),'Linewidth', 1.5)
 figure
  loglog(n(g),r2exp(g),'+', n(g),r2_ne_poly_eff(g), n(g),r2_ne(g),'Linewidth', 1.5)
```

```
    figure
    loglog(n(h),r2exp(h),'+', n(h),r2_ne_poly_eff(h), n(h),r2_ne(h),'Linewidth', 1.5)

    figure
    loglog(n(e),r2exp(e),'+', n(e),r2_dense_poly_eff(e), n(e),r2_dense(e),'Linewidth', 1.5)
   figure
    loglog(n(f),r2exp(f),'+', n(f),r2_dense_poly_eff(f), n(f),r2_dense(f),'Linewidth', 1.5)
   figure
    loglog(n(g),r2exp(g),'+', n(g),r2_dense_poly_eff(g), n(g),r2_dense(g),'Linewidth', 1.5)
    figure
    loglog(n(h),r2exp(h),'+', n(h),r2_dense_poly_eff(h), n(h),r2_dense(h),'Linewidth', 1.5)

    %plot(n(a),r2_dense_poly_eff(a),n(a),r2_ne_poly_eff(a), n(a), r2star_ne_poly_eff(a),'Linewidth', 1.5)
   return
   figure
   subplot(2,2,1), plot(n(a),r2exp(a),'+', n(a),r2_iso(a), n(a),r2_dense(a),n(a),r2_ne(a), n(a), r2star_iso(a),'Linewidth', 1.5)
   %xlim([0.5,100]), ylim([1,1000])
   xlabel('Number of IONC per nanoemulsion droplet')
   ylabel('Relaxivity r2 [mM-1 s-1]')
   title('p10 at 0.47 T')
   legend('Exp','Isotropic','Dense Aggregate','Loose Aggregate','Static')
   set(gca,'FontSize',textfont)

   subplot(2,2,3), plot(n(b),r2exp(b),'+', n(b),r2_iso(b), n(b),r2_dense(b),n(b),r2_ne(b), n(b), r2star_iso(b), 'Linewidth', 1.5)
   %xlim([0.5,100]), ylim([1,1000])
   xlabel('Number of IONC per nanoemulsion droplet')
   ylabel('Relaxivity r2 [mM-1 s-1]')
   title('p10 at 1.5 T')
```

```
   subplot(2,2,2), plot(n(c),r2exp(c),'+', n(c),r2_iso(c), n(c),r2_dense(c),n(c),r2_ne(c), n(c), r2star_iso(c), 'Linewidth',1.5)
   %xlim([0.5,100]), ylim([1,1000])
   xlabel('Number of IONC per nanoemulsion droplet')
   ylabel('Relaxivity r2 [mM-1 s-1]')
   title('p10 at 3 T')

   subplot(2,2,4), plot(n(d),r2exp(d),'+', n(d),r2_iso(d), n(d),r2_dense(d),n(d),r2_ne(d), n(d), r2star_iso(d), 'Linewidth',1.5)
   %xlim([0.5,100]), ylim([1,1000])
   xlabel('Number of IONC per nanoemulsion droplet')
   ylabel('Relaxivity r2 [mM-1 s-1]')
   title('p10 at 7 T')
   figure
   subplot(2,2,1), plot(n(a),r2exp(a),'+', n(a),r2_iso(a), n(a),r2_dense_poly_eff(a),n(a),r2_ne_poly_eff(a), n(a), r2star_ne_poly_eff(a),'Linewidth', 1.5)
   xlabel('Number of IONC per nanoemulsion droplet')
   ylabel('Relaxivity r2 [mM-1 s-1]')
   title('p10 at 0.47 T')
   legend('Exp','Isotropic','Dense Aggregate with polydisp','Loose Aggregate with polydisp','Static with polydisp')
   set(gca,'FontSize',textfont)
   subplot(2,2,3), plot(n(b),r2exp(b),'+', n(b),r2_iso(b), n(b),r2_dense_poly_eff(b),n(b),r2_ne_poly_eff(b), n(b), r2star_ne_poly_eff(b),'Linewidth', 1.5)
   xlabel('Number of IONC per nanoemulsion droplet')
   ylabel('Relaxivity r2 [mM-1 s-1]')
   title('p10 at 1.5 T')
   subplot(2,2,2), plot(n(c),r2exp(c),'+', n(c),r2_iso(c), n(c),r2_dense_poly_eff(c),n(c),r2_ne_poly_eff(c), n(c), r2star_ne_poly_eff(c),'Linewidth', 1.5)
   xlabel('Number of IONC per nanoemulsion droplet')
   ylabel('Relaxivity r2 [mM-1 s-1]')
   title('p10 at 3 T')
   subplot(2,2,4), plot(n(d),r2exp(d),'+', n(d),r2_iso(d), n(d),r2_dense_poly_eff(d),n(d),r2_ne_poly_eff(d), n(d), r2star_ne_poly_eff(d),'Linewidth', 1.5)
   xlabel('Number of IONC per nanoemulsion droplet')
   ylabel('Relaxivity r2 [mM-1 s-1]')
```

```
   title('p10 at 7 T')
   figure
   subplot(2,2,1), plot(n(e),r2exp(e),'+', n(e),r2_iso(e), n(e),r2_dense(e),n(e),r2_ne(e), n(e), r2star_iso(e),'Linewidth', 1.5)
   %xlim([0.5,100]), ylim([1,1000])
   xlabel('Number of IONC per nanoemulsion droplet')
   ylabel('Relaxivity r2 [mM-1 s-1]')
   title('p50 at 0.47 T')
   legend('Exp','Isotropic','Dense Aggregate','Loose Aggregate','Static')
   set(gca,'FontSize',textfont)

   subplot(2,2,3), plot(n(f),r2exp(f),'+', n(f),r2_iso(f), n(f),r2_dense(f),n(f),r2_ne(f), n(f), r2star_iso(f), 'Linewidth', 1.5)
   %xlim([0.5,100]), ylim([1,1000])
   xlabel('Number of IONC per nanoemulsion droplet')
   ylabel('Relaxivity r2 [mM-1 s-1]')
   title('p50 at 1.5 T')

   subplot(2,2,2), plot(n(g),r2exp(g),'+', n(g),r2_iso(g), n(g),r2_dense(g),n(g),r2_ne(g), n(g), r2star_iso(g), 'Linewidth',1.5)
   %xlim([0.5,100]), ylim([1,1000])
   xlabel('Number of IONC per nanoemulsion droplet')
   ylabel('Relaxivity r2 [mM-1 s-1]')
   title('p50 at 3 T')

   subplot(2,2,4), plot(n(h),r2exp(h),'+', n(h),r2_iso(h), n(h),r2_dense(h),n(h),r2_ne(h), n(h), r2star_iso(h), 'Linewidth',1.5)
   %xlim([0.5,100]), ylim([1,1000])
   xlabel('Number of IONC per nanoemulsion droplet')
   ylabel('Relaxivity r2 [mM-1 s-1]')
   title('p50 at 7 T')
```

```
   figure
   subplot(2,2,1), plot(n(e),r2exp(e),'+', n(e),r2_iso(e), n(e),r2_dense_poly_eff(e),n(e),r2_ne_poly_eff(e), n(e), r2star_ne_poly_eff(e),'Linewidth', 1.5)
   xlabel('Number of IONC per nanoemulsion droplet')
   ylabel('Relaxivity r2 [mM-1 s-1]')
   title('p50 at 0.47 T')
   legend('Exp','Isotropic','Dense Aggregate with polydisp','Loose Aggregate with polydisp','Static with polydisp')
   set(gca,'FontSize',textfont)
   subplot(2,2,3), plot(n(f),r2exp(f),'+', n(f),r2_iso(f), n(f),r2_dense_poly_eff(f),n(f),r2_ne_poly_eff(f), n(f), r2star_ne_poly_eff(f),'Linewidth', 1.5)
   xlabel('Number of IONC per nanoemulsion droplet')
   ylabel('Relaxivity r2 [mM-1 s-1]')
   title('p50 at 1.5 T')
   subplot(2,2,2), plot(n(g),r2exp(g),'+', n(g),r2_iso(g), n(g),r2_dense_poly_eff(g),n(g),r2_ne_poly_eff(g), n(g), r2star_ne_poly_eff(g),'Linewidth', 1.5)
   xlabel('Number of IONC per nanoemulsion droplet')
   ylabel('Relaxivity r2 [mM-1 s-1]')
   title('p50 at 3 T')
   subplot(2,2,4), plot(n(h),r2exp(h),'+', n(h),r2_iso(h), n(h),r2_dense_poly_eff(h),n(h),r2_ne_poly_eff(h), n(h), r2star_ne_poly_eff(h),'Linewidth', 1.5)
   xlabel('Number of IONC per nanoemulsion droplet')
   ylabel('Relaxivity r2 [mM-1 s-1]')
   title('p50 at 7 T')
```

```
%-------------------------------------------------------------%
function f = Langevin(mu, B0, T)

%function f = Langevin(mu, B0, T)

k = 1.38e-23; %J/K
x = (mu*B0)/(k*T);
f = coth(x) - 1/x;
%-------------------------------------------------------------%
```

```
%-------------------------------------------------------------%
function f = relaxivity_r2_outersphere(r,D,Beq,m);

% function f = R2_outersphere(r,f,D,Beq)
%
% r = magnetic sphere radius
% D = Water diffusion constant
% Beq = equatorial field of magnetic sphere
% m = mol Fe per unit volume of magnetic sphere
%
% All parameters must be in SI units!!

gamma = 2*pi*42.58e6; %rad/T water proton gyromagnetic ratio
a = 16/45; % constant factor for outer sphere theory.

tauD = r.*r./D;
domega = gamma.*Beq;


f = a .* domega.^2  .* tauD ./ m;
%-------------------------------------------------------------%
```

```
%-------------------------------------------------------------%
function f = relaxivity_r2star_static(Beq,m);

% function f = R2_outersphere(r,f,D,Beq)
%
% r = magnetic sphere radius
% D = Water diffusion constant
% Beq = equatorial field of magnetic sphere
% m = mol Fe per unit volume of magnetic sphere
%
% All parameters must be in SI units!!

gamma = 2*pi*42.58e6; %rad/T water proton gyromagnetic ratio
a = 2*pi/(3*sqrt(3)); % constant factor for static theory.

domega = gamma.*Beq;


f = a.*domega./ m;
%-------------------------------------------------------------%
```